Biofilm 9 (2025) 100242

Contents lists available at ScienceDirect

Biofilm

journal homepage: www.sciencedirect.com/journal/biofilm

RpoN mediates biofilm formation by directly controlling *vps* gene cluster and c-di-GMP synthetic metabolism in *V. alginolyticus*

Na Zhang [a,d], Yanhua Zeng [a], Jiachengzi Ye [a,c], Chuancao Lin [a,c], Xiaoxiao Gong [a,c], Hao Long [a], Haimin Chen [a,c], Zhenyu Xie [a,b,c,*]

[a] State Key Laboratory of Marine Resource Utilization in the South China Sea, Hainan University, Haikou, 570228, Hainan Province, China
[b] Hainan Provincial Key Laboratory for Tropical Hydrobiology and Biotechnology, Hainan University, Haikou, 570228, Hainan Province, China
[c] School of Marine Biology and Fisheries, Hainan University, Haikou, 570228, Hainan Province, China
[d] School of Life and Health Sciences, Hainan University, Haikou, 570228, Hainan Province, China

ARTICLE INFO

Keywords:
Vibrio alginolyticus
rpoN
Biofilm formation
Exopolysaccharides
c-di-GMP
Hypoxic metabolism

ABSTRACT

Vibrio alginolyticus is a prevalent pathogen in both humans and marine species, exhibiting high adaptability to various adverse environmental conditions. Our previous studies have shown that Δ*rpoN* formed three enhanced biofilm types, including spectacular surface-attached biofilm (SB), scattered pellicle biofilm (PB), and colony rugosity. However, the precise mechanism through which *rpoN* regulates biofilm formation has remained unclear. Based on the critical role of Vibrio exopolysaccharide (VPS) in biofilm formation, several genes related to the production and regulation of VPS were characterized in *V. alginolyticus*. Our findings from mutant strains indicated that VPS has complete control over the formation of rugose colony morphology and PB, while it only partially contributes to SB formation. Among the four transcriptional regulators of the *vps* gene cluster, *vpsR* and VA3545 act as promoters, whereas VA3546 and VA2703 function as repressors. Through transcriptome analysis and c-di-GMP concentration determination, VA0356 and VA3580 which encoded diguanylate cyclase were found to mediate the Δ*rpoN* biofilm formation. As a central regulator, *rpoN* governed biofilm formation through two regulatory pathways. Firstly, it directly bound to the upstream region of VA4206 to regulate the expression of the *vps* gene cluster (VA4206-VA4196). Secondly, it directly and indirectly modulated c-di-GMP synthesis gene VA3580 and VA0356, respectively, thereby affecting c-di-GMP concentration and subsequently influencing the expression of *vps* transcription activators *vpsR* and VA3545. Under conditions promoting SB formation, Δ*rpoN* was unable to thrive below the liquid level due to significantly reduced activities of three catalytic enzymes (ACK, ADH, and ALDH) involved in pyruvate metabolism, but tended to reproduce in air-liquid interface, a high oxygen niche compared to the liquid phase. In conclusion, both exopolysaccharide synthesis and oxygen-related metabolism contributed to Δ*rpoN* biofilm formation. The role of RpoN-mediated hypoxic metabolism and biofilm formation were crucial for comprehending the colonization and pathogenicity of *V. alginolyticus* in hosts, providing a novel target for treating *V. alginolyticus* in aquatic environments and hosts.

1. Introduction

Vibrios are ubiquitous and abundant in aquatic environments, and are autochthonous to the global ocean [1]. Members of the *Vibrio* genus have the fastest replication rates and excellent adaptability to various environments [2]. *Vibrio alginolyticus* is one of the most prevalent *Vibrio* species in coastal oceans and estuaries and is an opportunistic pathogen that infects both humans and marine organisms [3,4]. Biofilms play a critical role in allowing *V. alginolyticus* to survive, persist, and infect its host [4]. Mature biofilms are complex three-dimensional structures with water channels that embed bacterial communities in their extracellular products (e.g., extracellular polysaccharides, proteins, and DNA) [5,6]. Three types of biofilms are commonly observed under laboratory conditions: surface-attached biofilms (SB), pellicle biofilms (PB), and wrinkly spreader variants on solid substrates (i.e., colony rugosity). They differ in important ways, possibly because of their spatial distribution and differences in nutrient transport [7,8]. During biofilm formation, *Vibrio* exopolysaccharide (VPS) plays multiple roles, both as a

* Corresponding author. State Key Laboratory of Marine Resource Utilization in the South China Sea, Hainan University, Haikou, 570228, Hainan Province, China.
E-mail address: xiezyscuta@163.com (Z. Xie).

https://doi.org/10.1016/j.bioflm.2024.100242
Received 23 September 2024; Received in revised form 3 December 2024; Accepted 9 December 2024
Available online 15 December 2024

molecular glue responsible for cell-cell or cell-surface adhesion and as a structural component of biofilms, stratifying bacterial communities and establishing gradients of nutrients and metabolic waste [9]. Other polysaccharides such as levans also serve as nutrients for bacteria [10]. It has been reported that VPS production is a highly complex process involving many genes. Various signaling factors are involved in the regulatory network, including transcription factors [11], quorum sensing (QS) [12], Cyclic diguanylate (c-di-GMP) [13] and alternative sigma factors [14,15]. In bacteria, specific sigma subunits bind to core RNA enzymes to form RNA holoenzymes (RNAP) and participate in the initiation of gene transcription [16]. *rpoN*, the only member of the sigma-54 family, is a global regulator that requires an activator protein (bacterial enhancer-binding protein, bEBP) to activate the transcription of different sets of genes. Multiple bacterial bEBPs respond to different environmental signals [17].

It has been reported that in *Vibrio cholerae* RpoN participates in the quorum sensing (QS) system and activates *aphA* expression at low cell density (LCD), as well as *hapR* expression at high cell density (HCD) [18,19]. The *vps* gene cluster, responsible for the synthesis of extracellular polysaccharide (EPS) in *V. cholerae*, is regulated by two transcriptional activators: VpsR and VpsT [11,20–22]. HapR directly inhibits VpsT, thereby suppressing *vps* production and biofilm formation (Srivastava et al., 2012; [19,23]). c-di-GMP, a critical second messenger in bacteria, is regulated by cyclic diguanylate cyclases (DGCs) and phosphodiesterases (PDEs), facilitating the transition from a planktonic lifestyle to biofilm formation [24]. VpsR, once activated by c-di-GMP, forms a complex with it to reactivate VpsT [11]. HapR also indirectly inhibited VpsT by regulating c-di-GMP level [25].

Moreover, transcription of genes involved in c-di-GMP metabolism is controlled by sigma factors in various bacteria. In *Pseudomonas stutzeri*, *rpoN* acts as a central regulator by inducing RNA-binding protein RmsA to suppress *sadC* expression, encoding for DGC [26]. Additional, both PA4108 and PA4781 encoded PDE which dependent on *rpoN* in *Pseudomonas aeruginosa* [27]. Although the role of RpoN in regulating c-di-GMP in *Vibrio* spp. is not well-documented, it is reasonable to hypothesize that RpoN could modulate biofilm formation through its mediation of c-di-GMP levels, given its established regulatory functions in other bacteria. The genome of *V. alginolyticus* HN08155 contains an impressive 63 genes encoding enzymes involved in c-di-GMP metabolism and the overexpression of specific DGC-encoding genes (VA0356, VA1591 (*cdgM*), VA4033 (*dgcB*), and VA0088) significantly enhances biofilm formation [24]. Further research is required to elucidate the specific c-di-GMP genes influenced by RpoN, thus contributing to a comprehensive understanding of the intricate mechanism governing biofilm formation regulated by RpoN.

In addition to the specific expression of its components, metabolic remodeling in response to environmental factors also triggers the induction of biofilm formation ([28]; Shimada et al., 2021). The metabolism of amino acids, particularly arginine, has been reported to impact the formation of biofilms [29]. Most laboratory-biofilm cultures employ static or low-speed culture conditions, resulting in limited oxygen concentration that is crucial for respiration and fermentation metabolism. Oxygen concentration is relatively elevated at the air-liquid interface (ALI), a favorable ecological niche where bacteria use both nutrients and oxygen [7]. Oxygen drives bacteria towards the ALI, where they colonize and form biofilms. During this process, whether SB or PB is formed first depends on the species or strain. For example, SB and PB are predominant in *Dickeya dadantii* [30] and *Vibrio fischeri* [31], respectively.

Our previous study revealed that the absence of *rpoN* in *V. alginolyticus* HN08155 resulted in enhanced biofilm formation, including pellicle formation at ALI, surface-attached biofilm and a change in colony morphology from smooth to rugose [14]. To further elucidate the mechanism underlying *rpoN*-mediated regulation of biofilm formation, we characterized the gene cluster encoding biofilm-associated polysaccharides and their transcriptional regulators, as well as DGC-encoding genes implicated in Δ*rpoN* biofilm formation. Expanding upon the distinct contributions of polysaccharides to the three different types of biofilms and the observed differential growth state between Δ*rpoN* and WT, we conducted further discussion into the interplay among *rpoN*, oxygen-related metabolism, and biofilm formation.

2. Materials and methods

2.1. Strains and growth conditions

All strains and plasmids used in this study are listed in Table 1 and were routinely grown in LB medium (consisting of 1 % tryptone, 1 % NaCl, and 0.5 % yeast extract). *E. coli* β2163 was incubated at 37 °C in the presence of 0.3 mM DAP (diaminopimelic acid). *Vibrios* were cultured at 30 °C. *V. alginolyticus* HN08155 and Δ*rpoN* served as wild-type and *rpoN* deletion mutant strains, respectively, both of which were obtained from laboratory collections. Plasmid pDM4, which is resistant to chloramphenicol (Cm), was induced with 10 % sucrose. The plasmid pACYC184 harbors genes for resistance to both Cm and tetracycline (Tc), with the Tc gene being replaced by a target sequence in order to construct novel plasmids. The pEASY-Blunt E1 Expression vector, besides exhibiting ampicillin (Amp) resistance, possesses a histidine-tag and enables efficient expression of exogenous proteins in *Escherichia coli*. Antibiotics were used at the following concentrations: Amp, 100 μg/mL for *Vibrio* spp.; Cm, 20 μg/mL for the propagation of suicide plasmids in *E. coli* β2163 and 10 μg/mL for integrated plasmids in *Vibrios*.

2.2. Recombinant DNA techniques and genetic manipulations

High-fidelity DNA polymerase 2 × Phanta Max Mixture (Vazyme, Nanjing, China) was used for PCR amplification. To generate the deletion constructs, two DNA fragments of approximately 500 bp, containing the truncated gene and the upstream and downstream sequences, were assembled into the suicide plasmid pDM4. Ligation was performed using double-enzyme digestion with T4 DNA ligase (Thermo Fisher Scientific, Waltham, MA, USA). To generate overexpression constructs, a DNA ORF (open reading frame) fragment of the truncated gene was assembled into the expression plasmid pACYC184. Ligation was performed using a ClonExpress® Ultra One Step Cloning Kit (Vazyme, Nanjing, China). All constructed plasmids were introduced into *E. coli* β2163 by chemical transformation. Plasmids were mobilized by biparental mating using the donor *E. coli* β2163 strain. Briefly, cultures of the donor and recipient strains were mixed at a 1:1 ratio and co-cultured on LB agar plates (37 °C, 6 h). Transconjugants were selected on LB agar plates containing Cm^R and Amp^R. Single colonies were induced using 50 % sucrose. Genetic knockout mutant strains were confirmed using PCR. The overexpression strains were purified by scribing purification on double antibiotic plates (Cm^R and Amp^R).

2.3. Analysis of biofilm formation, static growth, and colony biofilm formation

Strains stored at -80 °C were cultured at 30 °C using the plate-streaking technique. Single colonies were inoculated into LB liquid medium and grown overnight at 30 °C and 180 rpm, then transferred into 50 mL of fresh LB medium and shaken for 2–3 h. Bacteria in a vigorous growth state were adjusted to an $OD_{600nm} = 0.6$ (as adjusted medium), and then the resulting bacterial suspension was diluted 1:100 into 50 mL of fresh LB medium, as diluted medium.

Biofilm formation assays included qualitative analysis of the PB and quantitative analysis of the SB. Aliquots of 200 μL of **diluted medium** were added to each well of the 96-well micro-plate. Each strain had five wells for parallel experiments. The 96-well microplates were incubated at 30 °C without shaking. Quantitative analysis of SB was performed at 6 and 24 h. The bacterial solution was removed, washed twice with

Table 1
Bacterial strains and plasmids used in this study.

Strain or plasmid	Description	Reference or source
Strain		
Vibrio alginolyticus		
HN08155	Wild-type, WT; Amp^r	Laboratory collection
ΔVA4206	in-frame deletion in gene VA4206; Amp^r	This study
ΔVA4202	in-frame deletion in gene VA4202; Amp^r	This study
Δ*vpsR*	in-frame deletion in gene *vpsR*; Amp^r	This study
ΔVA2703	in-frame deletion in gene VA2703; Amp^r	This study
ΔVA3545	in-frame deletion in gene VA3545; Amp^r	This study
ΔVA3546	in-frame deletion in gene VA3546; Amp^r	This study
Δ*rpoN*VA4206	in-frame deletion in gene *rpoN* and VA4206; Amp^r	This study
Δ*rpoN*VA4202	in-frame deletion in gene *rpoN* and VA4202; Amp^r	This study
Δ*rpoN*v*psR*	in-frame deletion in gene *rpoN* and *vpsR*; Amp^r	This study
Δ*rpoN*VA2703	in-frame deletion in gene *rpoN* and VA2703; Amp^r	This study
Δ*rpoN*VA3545	in-frame deletion in gene *rpoN* and VA3545; Amp^r	This study
Δ*rpoN*VA3546	in-frame deletion in gene *rpoN* and VA3546; Amp^r	This study
ΔVA0356	in-frame deletion in gene VA0356; Amp^r	This study
Δ*rpoN*VA0356	in-frame deletion in gene *rpoN* and VA3546; Amp^r	This study
ΔVA3580	in-frame deletion in gene VA3580; Amp^r	This study
Δ*rpoN*VA3580	in-frame deletion in gene *rpoN* and VA3580; Amp^r	This study
ΔΔΔ	in-frame deletion in three genes (*rpoN*, VA3546 and VA3580); Amp^r	This study
Δ*rpoN*VA0461	in-frame deletion in gene *rpoN* and VA0461; Amp^r	This study
Δ*rpoN*VA0663	in-frame deletion in gene *rpoN* and VA0663; Amp^r	This study
Δ*rpoN*VA2417	in-frame deletion in gene *rpoN* and VA2417; Amp^r	This study
Δ*rpoN*VA2972	in-frame deletion in gene *rpoN* and VA2972; Amp^r	This study
Δ*rpoN*VA4030	in-frame deletion in gene *rpoN* and VA4030; Amp^r	This study
Δ*rpoN*VA4418	in-frame deletion in gene *rpoN* and VA4418; Amp^r	This study
E. coli		
β2163	Δ*dapA*::(erm-pir)	Laboratory collection
Rosetta-E1-RpoN	Efficient expression of RpoN induced by IPTG; Amp^R	This study
Plasmids		
pDM4	Suicide vector, *pir* dependent; R6K *sacBR* Cm^r	Laboratory collection
pACYC184	Expression vector; Cm^r and Tc^r	Laboratory collection
pEASY-Blunt E1 Expression vector	Efficient expression of target protein; his-tag; Amp^R	#CE111, TransGen Biotench, China

phosphate buffered saline (PBS), dried, stained for 30 min with 0.1 % crystal violet, and dissolved in 95 % ethanol for 2 h. Light absorption was measured at 570 nm using a multi-label plate reader (BioTek, Vermont, USA). Qualitative analysis of the PB was performed at 6 and 24 h.

The static growth ability assay was performed using the same 96-well microplate that was statically incubated at 30 °C for 24 h in a multi-label plate reader. The absorption value at 600 nm was measured every hour, and Microsoft Excel was used for graph analysis.

The colony biofilms used for qualitative analysis were prepared from cultures inoculated with five single colonies grown overnight at 30 °C without shaking. The **adjusted medium** was concentrated from 500 mL to 10 μL, and 5 μL was spotted onto LB agar plates. Once the spots were dried, the plates were incubated at 30 °C for 14 h and imaged.

2.4. Image analyses of microscopy

Briefly, a 12-well micro-plate containing diluted medium was statically cultured at 30 °C. Each well contained 2 mL of medium and a sloped cover glass. After with drawing the liquid, samples collected at 6 and 24 h were sequentially treated with 2.5 % glutaraldehyde for 2 h, 1 mg/mL FITC-ConA for 30 min to label EPS, and 1 mg/mL propidium iodide (PI) for 30 min to label nucleic acids. Subsequently, the coverslips were imaged under a microscope (Leica Microsystems).

2.5. Enzyme activity assay

Catalyzing enzyme activities (e.g., ADH, ALDH, and ACK) were assessed using commercially available kits (Comin, Suzhou, China). Briefly, all three enzymes catalyze the transition between NAD^+ and NADH, and the catalytic activity of these enzymes can be characterized by measuring the amount of NADH that changes the light absorption value over a certain period. The light absorption wavelength of NADH was 340 nm. The sample was a colony biofilm with a tissue-calculated weight. One unit of enzyme activity was defined as the amount of enzyme that changed 1 mol NADH in 1 min under the assay conditions.

2.6. Transcriptomic and qRT-PCR analyses

Relative expression levels of key genes involved in biofilm formation were determined using RNA-Seq and quantitative real-time PCR (qRT-PCR). It is difficult to collect samples because a large amount of biofilm is attached to the surface of the liquid medium and the wall of microplate. Total RNA was prepared according to the culture method used for the **colony biofilm** assay. Bacterial cells [e.g., wild-type (WT) and Δ*rpoN*] were collected by cell-scraper. Each set of four colonies was combined to form a single sample, and three independent groups were established with a total of 12 colonies per strain. Subsequently, the bacterial cells were rapidly frozen in liquid nitrogen and stored at -80 °C. Total RNA was extracted using an RNA extraction kit (Tiangen, Beijing, China), and 2 % agarose gel electrophoresis was performed at 150 V for 20 min. The results showed three clear bands without dragging. RNA quality was determined by NanoPhotometer® NP80 (IMPLEN, München, Germany) for subsequent experiments. The HiScript II Q RT SuperMix for qPCR (Vazyme, Nanjing, China) was used for reverse transcription. The ChamQ Universal SYBR qPCR Master Mix (Vazyme, Nanjing, China) was used for qRT-PCR. The samples were collected using the same protocol as for the qRT-PCR assay. However, to ensure data availability, four sets of 16 colonies were collected in parallel for each strain. RNA-seq analysis was performed using the Majorbio Cloud platform (www.majorbio.com). Original transcriptome data were submitted to the NCBI for Biotechnology Information database (BioProject ID: PRJNA1030980).

2.7. Extraction and measurement of intracellular c-di-GMP

The intracellular c-di-GMP concentration of bacteria in colony biofilm was determined. After adjusting the bacterial concentration to $OD_{600nm} = 0.6$, a 1.5 mL bacterial solution was centrifuged at 13000 rpm for 3 min and resuspended in 30 μL LB medium. Each colony was formed using 6 μL of the resuspension, with a total of four colonies on each plate and four parallel plates in total. Three plates were used for c-di-GMP extraction, while one plate was used for determination of total

bacterial protein (using the BCA Protein Concentration Assay kit). The extraction and quantification of c-di-GMP were conducted following the protocol described by Jones (2015). The extraction solution consisted of 100 mL of a mixture containing 40 % acetonitrile, 40 % methanol, 19.9 % ultrapure water, and 0.1 % formic acid. Four colonies were collected into a sterile centrifuge tube using a sterile scraper. Then, 1 mL of the extract along with three enzyme-free steel beads were added to the tube and crushed for 240 s using a tissue crusher. Due to the difficulty in breaking Δ*rpoN* colony, efforts were made to break it as long as possible to achieve homogeneity without agglomeration. Subsequently, the sample was allowed to stand at -20 °C for 30 min followed by centrifugation at 13000 rpm for 10 min. The supernatant (900 μL) was transferred into a new 50 mL centrifuge tube and freeze-dried for 12 h. The resulting dried powder was reconstituted in sterile ultrapure water (1 mL), and the concentration of c-di-GMP was determined using high-performance liquid chromatography (PM1000, China).

High performance liquid chromatograph using solvent A (0.1 % acetic acid soluble in 10 mM ammonium acetate) and solvent B (0.1 % formic acid in methanol). The measurement procedure and flow rate were as follows: time (t) = 0–5 min, 98 % A + 2 % B; t = 5–10 min, 95 % A + 5 % B; t = 10–15 min, 90 % A + 10 % B; t = 15–20 min, 10 % A + 90%B; t = 20–25 min, 98 % A + 2%B. Apart from 0 to 5 min flow rate is 0.5 mL/min, the rest are 0.3 mL/min. To determine the cyclic diguanosine acid standard curve, 1 μmol of the purchased standard (#C057, Biolog) was dissolved in 1 mL of sterile ultrapure water (concentration of 1 mM), and then diluted to 0.1 mM, 50 μM, 25 μM, 12.5 μM, 6.25 μM, 3.125 μM, respectively. According to the peak interval of the sample, similar standards were selected for constructing the standard curve. Total bacterial protein was utilized for intracellular content homogenization of c-di-GMP concentration.

2.8. Electrophoretic mobility shift assay

Firstly, an *rpoN* expression vector should be constructed, connecting the open reading frame of *rpoN* and pEASY-Blunt E1 Expression vector, and chemically transformed in Rosetta cells, resulting in the formation of Rosetta-E1-*rpoN*. Subsequently, protein expression can be induced by adding IPTG at a final concentration of 1 mM. Extraction and purification of the *rpoN* protein by the His labeled protein micropurification kit (#220542, Bingene). Due to a high concentration of imidazole affect the effect of the combination of protein and DNA probe, the eluent would be replaced for PBS buffer using 10 kDa ultrafiltration tube. The concentration of RpoN was 2.142 mg/mL. Referring to the RpoN-binding site sequence in *V. cholerae* [32]: tGG(-24)cacnntttTGC(-12), MEME software (http://meme-suite.org/tools/meme) was used to explore potential binding sites for RpoN in the *V. alginolyticus* HN08155 genome. The biotin labeling potential binding sites were utilized for DNA probe in subsequent gel migration experiments. In brief, protein and DNA probe interactions were detected using a Chemiluminescent EMSA Kit (#GS009, Beyotime). With minor modifications according to the manufacturer's instructions, the free probe and bound bands were separated by electrophoresis using 6 % non-denaturing gel. UV crosslinking and incubation with HRP antibody were performed to visualize the position of the probe through exposure.

2.9. Statistical analysis

Data are presented as the mean ± standard deviation (S.D.). Statistical analyses were performed using GraphPad Prism 9 software (Version 9.0.0). $p<0.05$ was considered statistically significant. *p<0.05; **p<0.01; ***p<0.001; ****p<0.0001; ns, not significant. And the letters (a, b, c and d) represented statistically significant differences between samples, while identical letters indicate no significant.

3. Results

3.1. Transcriptome overview

Transcriptome sequencing was performed using colony biofilms of WT and Δ*rpoN*, which were cultured on LB plates for 14 h. The advantages of this particular biofilm lie in its significant disparity, phenotypic stability, and convenience for sample collection. The quality control data statistics are listed in Table S1. High-quality clean reads were obtained after quality cutting, ranging from 23,546,596 to approximately 27,436,366. The number of clean bases (bp) ranged from 3,306,297,433 to around 3,819,422,262, and the error rate was stable at 0.025 %. More than 99 % of the reads mapped to the genome. Correlation analysis revealed that there was a strong intercorrelation within each group of the four samples, while the correlation between different groups was relatively weak (Fig. 1A). Default parameters were used: p_{adjust} (corrected p-value) < 0.05 & $|\log2FC| \geq 1$. In comparison to WT, Δ*rpoN* showed significant up-regulation in 332 genes and down-regulation in 239 genes (Fig. 1B). KEGG enrichment analysis (Fig. 1C) in the down-regulation pathway of Δ*rpoN* showed terms for 'Biofilm formation-*Pseudomonas aeruginosa*,' 'Flagellar assembly,' 'Lipopolysaccharide biosynthesis,' etc. All nine genes involved in the biofilm synthesis pathway of *P. aeruginosa* belong to the type VI secretory system (T6SS). Transcriptomic analysis of *V. alginolyticus* also showed that *rpoN* is required for T6SS and flagella synthesis, which are two conserved phenomena in *Vibrio* [32–37]. Furthermore, we also reported specific pathways related to metabolism, such as glyoxylate, dicarboxylate, and pyruvate metabolism.

Only two pathways exhibited significant up-regulation in Δ*rpoN*: 'Valine, leucine, and isoleucine degradation' and 'ABC transporters' (padjust <0.05) (Fig. 1D). Within the valine, leucine, and isoleucine degradation pathway, a majority of differentially expressed genes were enriched in methylmalonate semialdehyde synthesis, methylmalonate semialdehyde conversion to acetyl-CoA. This suggests that branched chain amino acids may serve as an important energy source in Δ*rpoN*. Among the ABC transporter-oligosaccharide transport system components responsible for Maltose/Maltodextrin transportation (VA4207 MalK, VA4208 MalE, VA4209 MalF, and VA4210 MalG), which were fully mapped in the genome, showed significant upregulation in Δ*rpoN* transcriptome. Further analysis of adjacent genomic regions revealed a cluster of 11 genes (VA4206-VA4196) encoding vibrio polysaccharide synthesis (VPS) that also displayed increased transcript levels in Δ*rpoN*. To investigate whether *vps* gene cluster was involved in biofilm formation by Δ*rpoN* detailed homology analysis and deletion mutation verification were conducted.

3.2. VPS-activated pellicle formation and colony rugosity in ΔrpoN

The *vps* gene cluster was located at *V. alginolyticus* HN08155 Chromosome2 was composed of 11 contiguous genes transcribed in the same direction (Fig. S1), which were highly homologous to *vps* of *V. cholerae*, *cps* of *V. parahaemolyticus*, and *brp* of *V. vulnificus*. The functional annotations of the gene clusters are listed in Table S2. The original gene VA4206, which encodes undecaprenyl-phosphate glucose phosphotransferase, is homologous to *vpsL* of *V. cholerae*, *cpsA* of *V. parahaemolyticus* and *wcaJ* of *E. coli* (Fig. S2A). The phylogenetic tree based on the amino acid sequence showed that *V. alginolyticus* VA4206 was 100 % similar to *V. paraholyticus* CpsA and 98 % similar to *V. cholerae* VpsL, which clustered into a branch with *E. coli* WcaJ under the pressure of VpsM as a foreign gene. The evolutionary level of WcaJ is relatively distant compared with other *Vibrios*. Transcriptome sequencing results indicated that almost the entire *vps* gene cluster was up-regulated in Δ*rpoN* (Fig. 2A). Therefore, VA4206, the starting gene and VA4202 with the highest transcriptional abundance in the whole gene cluster as the representative were selected to construct single deletion mutant strains (ΔVA4206 and ΔVA4202) and double deletion

mutant strains (Δ*rpoN*VA4206 and Δ*rpoN*VA4202). Unlike the rugose colony morphology in Δ*rpoN*, both Δ*rpoN*VA4206 and Δ*rpoN*VA4202 exhibited a smooth phenotype similar to WT (Fig. 2C), which suggested that the *vps* gene cluster played a crucial role in regulating colony morphology.

After 6 h of static incubation, the WT formed an obvious SB at the air-liquid interface (AIL) of the microplate wall (Fig. 2E), which could be stained with crystal violet as a purple ring. The biofilm biomass of WT,

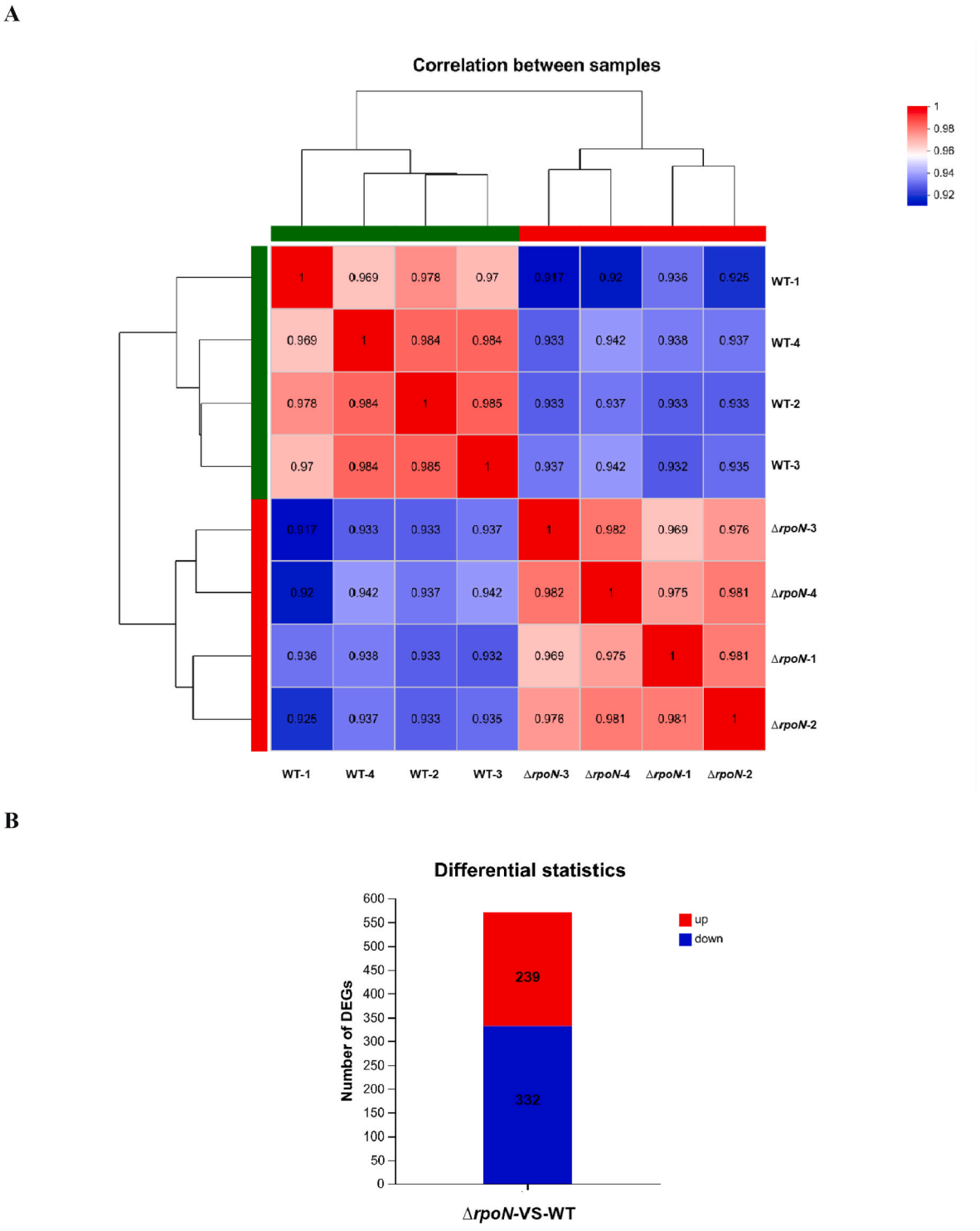

Fig. 1. Transcriptome analysis between WT and Δ*rpoN*. (A). Correlation analysis. Sample names and sample clustering are located on the right/bottom and top/left, respectively. The squares with different colors represent the correlation level of the two samples. Where the value is the correlation coefficient of the two samples, the larger the value, the greater the correlation between the two samples, the more similar. (B). Statistical summary of DEGs numbers. The Red and Blue column denotes up-regulated and down-regulated DEGs in the treatment group compare with the control group, respectively. (C) and (D) were KEGG enrichment analysis of down-regulated and up-regulated in Δ*rpoN* vs WT. The top 20 enriched pathways with the minimum q value are displayed. The size of the dot is proportional to the number of DEGs. Padjust is corrected P-value, ranging from 0 to 1; the closer the Padjust is to 0, the greater the extent of enrichment. Generally, Padjust <0.05 is considered as a significant enrichment item. (For interpretation of the references to color in this figure legend, the reader is referred to the Web version of this article.)

C

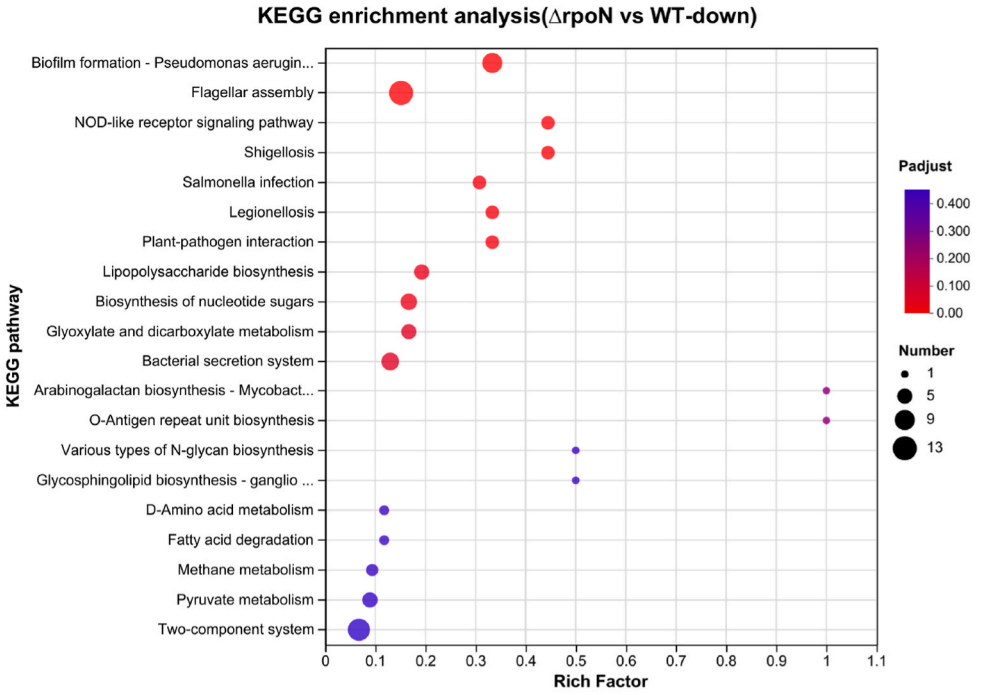

D

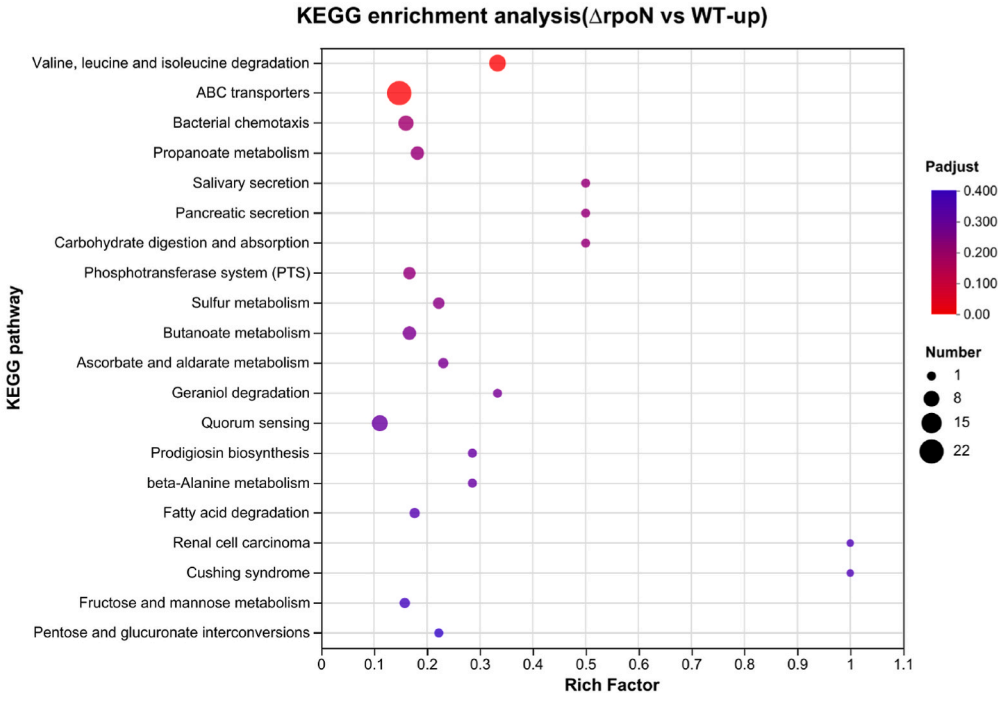

Fig. 1. (*continued*).

ΔVA4206 and ΔVA4202, as determined by OD_{570nm} values, were 2.29, 0.85 and 0.92, respectively (Fig. 2F). Thus, the absence of either VA4206 or VA4202 significantly reduced the ability of *V. alginolyticus* biofilm formation ($p < 0.01$). However, all mutants containing *rpoN*, including Δ*rpoN*, exhibited a lack of biofilm formation due to their sluggish growth during the initial stage of culture ($OD600_{nm} \approx 0.3$ at 6 h). At 24 h, the biofilm of the WT was dispersed ($OD_{570nm} = 0.10$). The mutants ΔVA4206 and ΔVA4202 were similar to WT, with no biofilm remaining

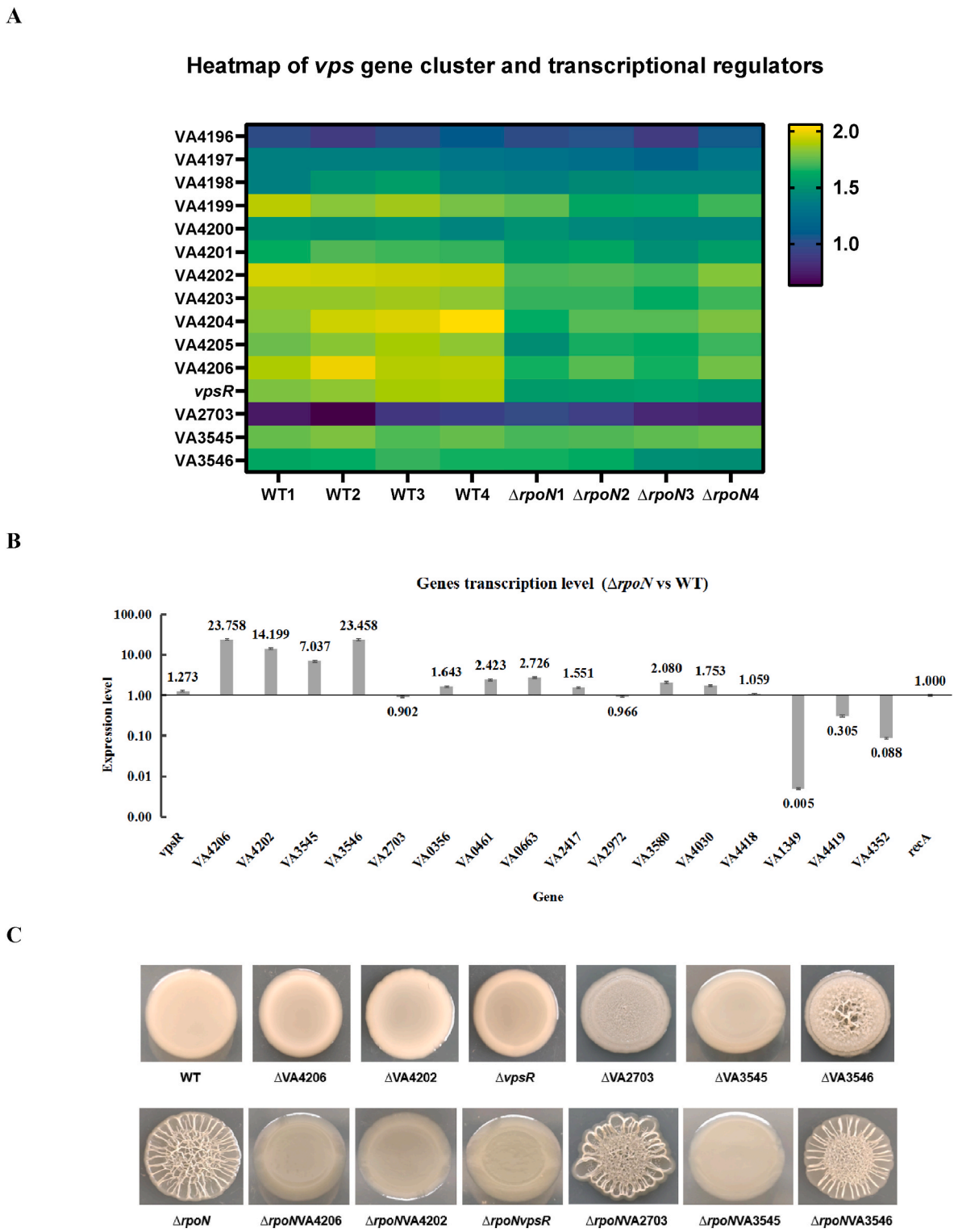

Fig. 2. Biofilm phenotypes associated with *vps* gene clusters and regulators. (A). Heat map of *vps* gene cluster and transcriptional regulators. In the transcriptome, yellow and blue indicated relatively high and low expression levels, respectively. (B) Genes transcript levels were quantified by qPCR in WT and Δ*rpoN*. *RecA* was used as reference gene whose expression was normalized as 1. Other genes were relative multiples of *recA*. The ordinate displayed the logarithm of the value that were homogenized by formula 2^(-ΔΔ). *RecA* = 1 was the intersection of the horizontal and vertical axes. The closer to 100 and 0, up- and down-regulation more significant, respectively. Error bars represent the standard deviation of triplicate samples. (C). Morphological images of colony biofilms. Bacteria were incubated for 14 h at 30 °C in LB-plate medium. (D). Pellicle biofilm was imaged at 24 h. (E). SB stained with crystal violet at 24 h. The absorbance values measured at 595 nm after 6 h and 24 h of crystal violet, denoted as (F) and (G) respectively, represented the quantification of SB formation. (H). Microscopic images of 24 h SB on coverslips after fluorescent staining with PI and Concanavalin-A. Except for WT, which was photographed at 40 × field of view (Bar = 10 μm), other strains were photographed at 5 × field of view (Bar = 100 μm). The first column was the superimposed channel; the second column was bright field channel (BF); the third column was green fluorescence after canavalin-A staining polysaccharide (FLUO-FITC); the fourth column was red fluorescence after PI staining nucleic acid (FLUO-Y3). (I). A potential binding site for *rpoN* located in the upstream region of VA4206. Red square represented potential binding site under the genome, indicating transcription in the same

direction as VA4206, a arrow points to the left. (J). The binding of *rpoN* to the putative binding site of VA4206 upstream by EMSA. RpoN: the purified protein RpoN, concentration was 2.142 mg/mL. VA4206: a potential rpoN binding site upstream of VA4206, labeled with biotin, concentration was 8.10 ng/μL. The upper band represented the protein-DNA binding complex. The lower band corresponds to the unbound DNA probe. In lanes 1 and 2, a low concentration of RpoN protein was used, with each lane receiving a volume of 2 μL. For lanes 3 and 4, the volume of RpoN protein was 4 μL, while the volume of ddH_2O was correspondingly decreased by 2 μL to ensure that the total volume of the system remained constant. The augmentation of RpoN protein levels resulted in the appearance of a distinct binding band, indicative of a DNA-protein complex, referred to as the Bound probe. Additionally, with a fixed quantity of DNA probe, the intensity of the binding band intensified, while the free probe band diminished in prominence, in correlation with the elevated amount of RpoN protein. (For interpretation of the references to color in this figure legend, the reader is referred to the Web version of this article.)

(Fig. 2D and E). At this time point, Δ*rpoN* formed SB and PB with complex extracellular matrices, whereas the double knockout mutants Δ*rpoN*VA4206 and Δ*rpoN*VA4202 failed to form PB (Fig. 2D) but still formed visible SB on the plate wall (Fig. 2E). The biofilm biomass of Δ*rpoN*, Δ*rpoN*VA4206 and Δ*rpoN*VA4202, as determined by OD_{570nm} values, were 3.70, 1.70 and 1.63, respectively (Fig. 2G). Fluorescence staining microscopy results at 24 h (Fig. 2H) showed that Δ*rpoN* formed a multi-layered reticular membrane structure with abundant biomass. The WT strain only formed microcolonies, and few bacteria gathered and adhered to the slide. Although the biofilm of Δ*rpoN*VA4206 was not similar to Δ*rpoN*, there were still cell aggregates (red fluorescence) that formed a band-shape SB.

A prospective binding site for RpoN, with the sequence TGCTAATTTTAAGCCAA, has been pinpointed 1233 base pairs upstream of the VA4206 gene. This site was also present inside VA4207, transcribed in the same orientation as VA4206 (Fig. 2I). EMSA analysis provided further validation of this binding site. An increase in the total RpoN protein levels led to the appearance of DNA-protein specific binding bands, demonstrating that RpoN was capable of binding to this potential site (Fig. 2J). The overall findings suggested that RpoN could directly bind upstream of the *vps* gene cluster to regulate VPS synthesis which was primarily controlling the development of rugose colonies and pellicles (PB), while also playing a partial role in SB formation.

3.3. RpoN indirectly regulated four transcriptional regulators of vps gene cluster

VpsR and VpsT have been shown to be positive regulators of biofilm formation in *V. cholerae* [23]. Based on the protein crystal structure and conserved amino acid residue sequences, four homologous VpsT proteins were identified in *V. parahaemolyticus*. The two biofilm activators were CpsQ (VPA1446) and ScrO (VPA0358), the biofilm inhibitor CpsS (VPA1447), and the non-essential factor ScrP (VP2710) [38]. Based on amino acid sequence homology, one VpsR homolog (VA0488) and three VpsT homologs (VA2703, VA3545, and VA3546) were retrieved from the genome of *V. alginolyticus* HN08155. A phylogenetic tree based on amino acid sequences showed that *V. alginolyticus* VpsR had 100 % and 98 % homology with *V. parahaemolyticus* and *V. cholerae,* respectively (Fig. S2B). However, VpsT is relatively complex. VA3545,VA3546, and VA2703 were similar to CpsQ, CpsS, and ScrP, respectively, and were independently aggregated into a compact branch. VA3546 showed 99 % similarity to *V. cholerae* VpsT. Under the pressure of VA3546, VA3545, and VA2703 converged into a single branch, which was far away from VA3546 (Fig. S2C). To explore the regulatory role of these four genes in biofilm formation and their relationship with RpoN, single gene deletion mutant strains (Δ*vpsR*, ΔVA2703, ΔVA3545, and ΔVA3546) and double gene deletion mutant strains (Δ*rpoNvpsR*, Δ*rpoN*VA2703, Δ*rpoN*VA3545, and Δ*rpoN*VA3546) were constructed.

The colony morphology of Δ*vpsR*, ΔVA3545, Δ*rpoNvpsR* and Δ*rpoN*VA3545 appeared smooth, while ΔVA2703, ΔVA3546, Δ*rpoN*VA2703 and Δ*rpoN*VA3546 were characterized by rugose colonies (Fig. 2C). At 6 h compared to WT, both Δ*vpsR* and ΔVA3545 had decreased SB ($p < 0.01$), whereas ΔVA2703 and ΔVA3546 showed a slight increased SB (Fig. 2F). And the SB of ΔVA3546 was maintained to the end without detaching (Fig. 2G). At 24 h, compared to Δ*rpoN*, there was a significant decrease in biofilm formation for Δ*rpoNvpsR* and Δ*rpoN*VA3545, with a shallow SB ($p < 0.01$) and disappearance of PB (Fig. 2D and G). Fluorescence staining showed that SB formed by Δ*rpoNvpsR* was similar to that of Δ*rpoN*VA4206 (Fig. 2H). Based on these results, *vpsR* and VA3545 were active transcription factors involved in biofilm formation, whereas VA3546 and VA2703 act as inhibitors.

Although RpoN binding sites had not been identified in the upstream areas of the four regulators, significantly higher expression levels of *vpsR*, VA3545 and VA3546 were observed in Δ*rpoN* (Fig. 2B). These findings suggested that *rpoN* regulated biofilm formation through its indirectly regulation of *vpsR* and VA3545, and neither *vpsR* nor VA3545 could be substituted for each other. However, VA3546, as a biofilm inhibitor, was significantly upregulated in Δ*rpoN* but did not exert the inhibiting effect of biofilm formation. In addition, there was no significant difference in the expression of VA2703 (Fig. 2B), which was unaffected by *rpoN*.

3.4. RpoN controlled intracellular c-di-GMP levels through direct and indirect regulation of c-di-GMP synthesis gene VA3580 and VA0356, respectively

Although RopN was capable of directly binding to the upstream region of VA4206, its regulation appeared to be distal. And *rpoN* indirectly influenced the transcriptional regulators of *vps*, which potentially resulted in a weaker regulatory effect on *vps* by *rpoN*. In *V. cholerae*, both VpsR and VpsT function as c-di-GMP effectors that rely on c-di-GMP for regulating downstream *vps* gene cluster. The intracellular second messenger c-di-GMP plays a promoting role in biofilm formation. The contribution of genes encoding DGC in Δ*rpoN* robust biofilms was characterized through transcriptome analysis. There were significant up-regulation of 8 genes involved in c-di-GMP synthesis (VA0356, VA0441, VA0663, VA2417, VA2972, VA3580, VA4030, and VA4418) in Δ*rpoN* (Fig. 3A). Construction of double gene mutations showed that Δ*rpoN*VA3580 significantly altered the rugose morphology while Δ*rpoN*VA0356 only slightly affected it, however, neither completely restored smoothness (Fig. 3B). This suggested that the synthetic genes may have a synergistic effect on c-di-GMP level. Further triple mutation analysis (strain ΔΔΔ) involving *rpoN* along with VA0356 and VA3580 resulted in a completely smooth colony morphology and a obvious reduced SB (Fig. 3B and C), indicating that both VA0356 and VA3580 play major roles in Δ*rpoN* c-di-GMP synthesis.

The sequences of VA0356 and VA3580 were characterized. VA0356 (1881 bp, 626 aa) which encodes a fusion protein consisting of transmembrane region - Cache - PAS - PAC - GGDEF multidomains (Fig. 3D). The Cache region is an extracellular domain that plays a role in the recognition of small molecules and is influenced by calcium ion channel subunit proteins and chemotactic receptors. The adjacent genes from VA0348 to VA0356 were oriented in the same transcriptional direction (Fig. S5A). Notably, the expression levels of VA0352 to VA0356 were significantly up-regulated in Δ*rpoN*. Specifically, VA0352 functions as a transcription regulator *leuO* that was regulated by *ompA*, both of which affect biofilm formation [39]. Additionally, VA0353 encoded long-chain fatty acid-CoA ligase, while VA0354 and VA0355 encode acetolactate synthase large and small subunits respectively. In contrast, both VA0357 and VA0358 were transcribed in the opposite direction from VA0356; they respectively encoded a GntR family transcription regulator and

D

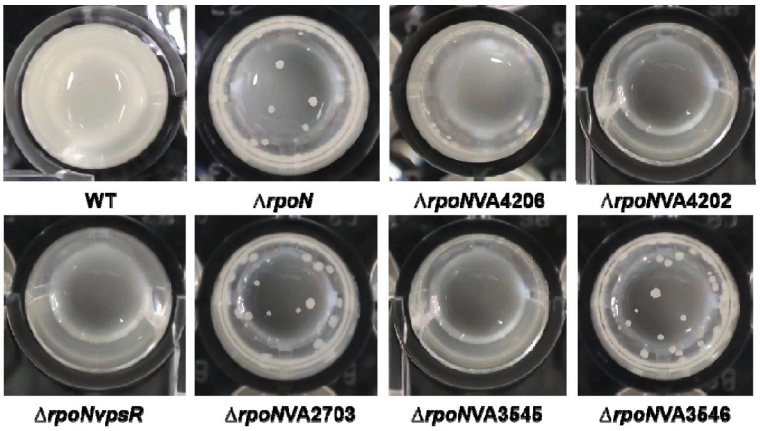

E

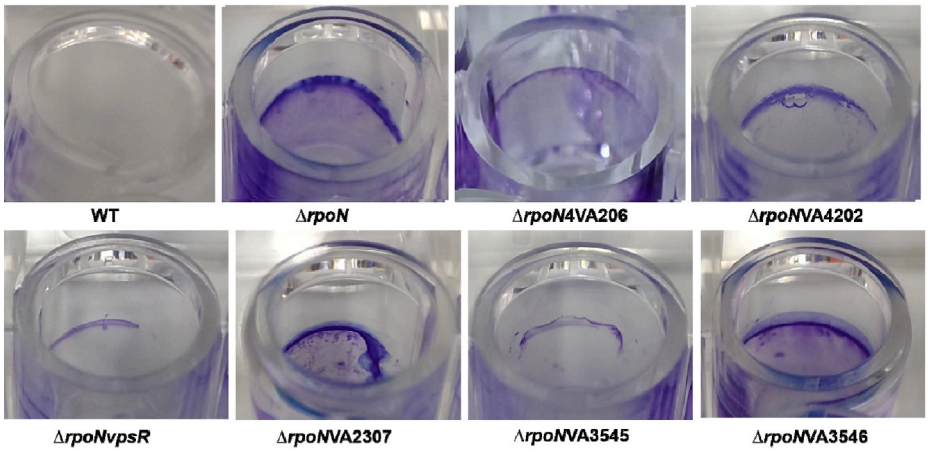

F

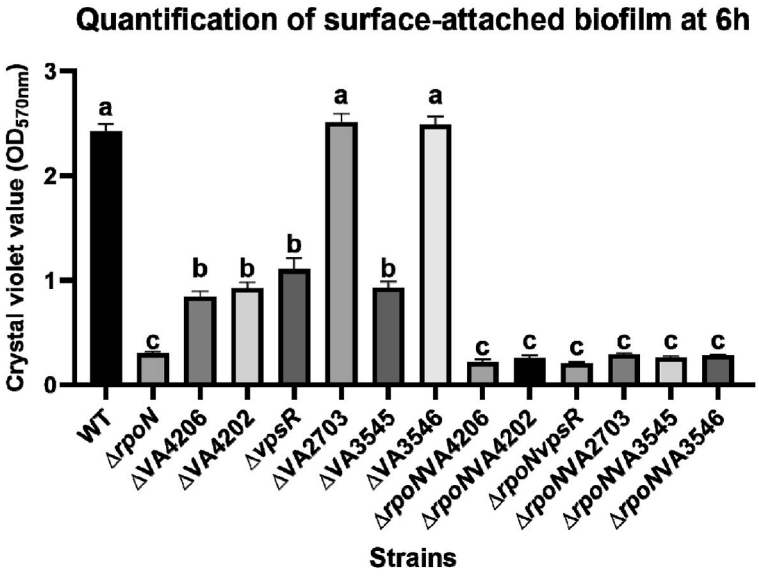

Fig. 2. (*continued*).

G

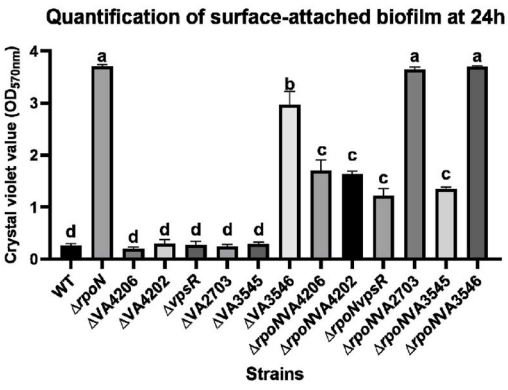

H

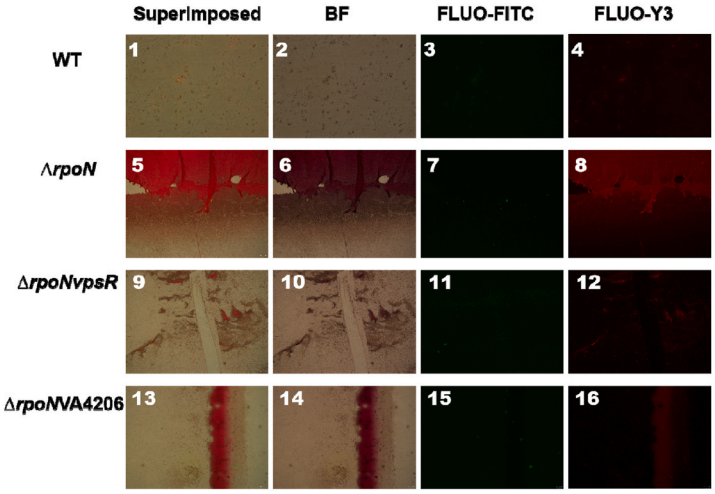

I

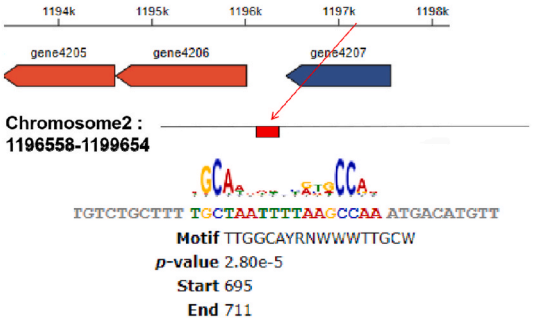

J

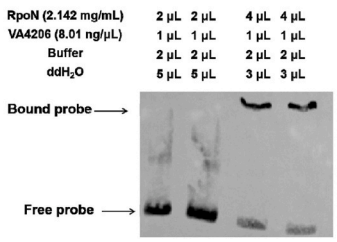

Fig. 2. (*continued*).

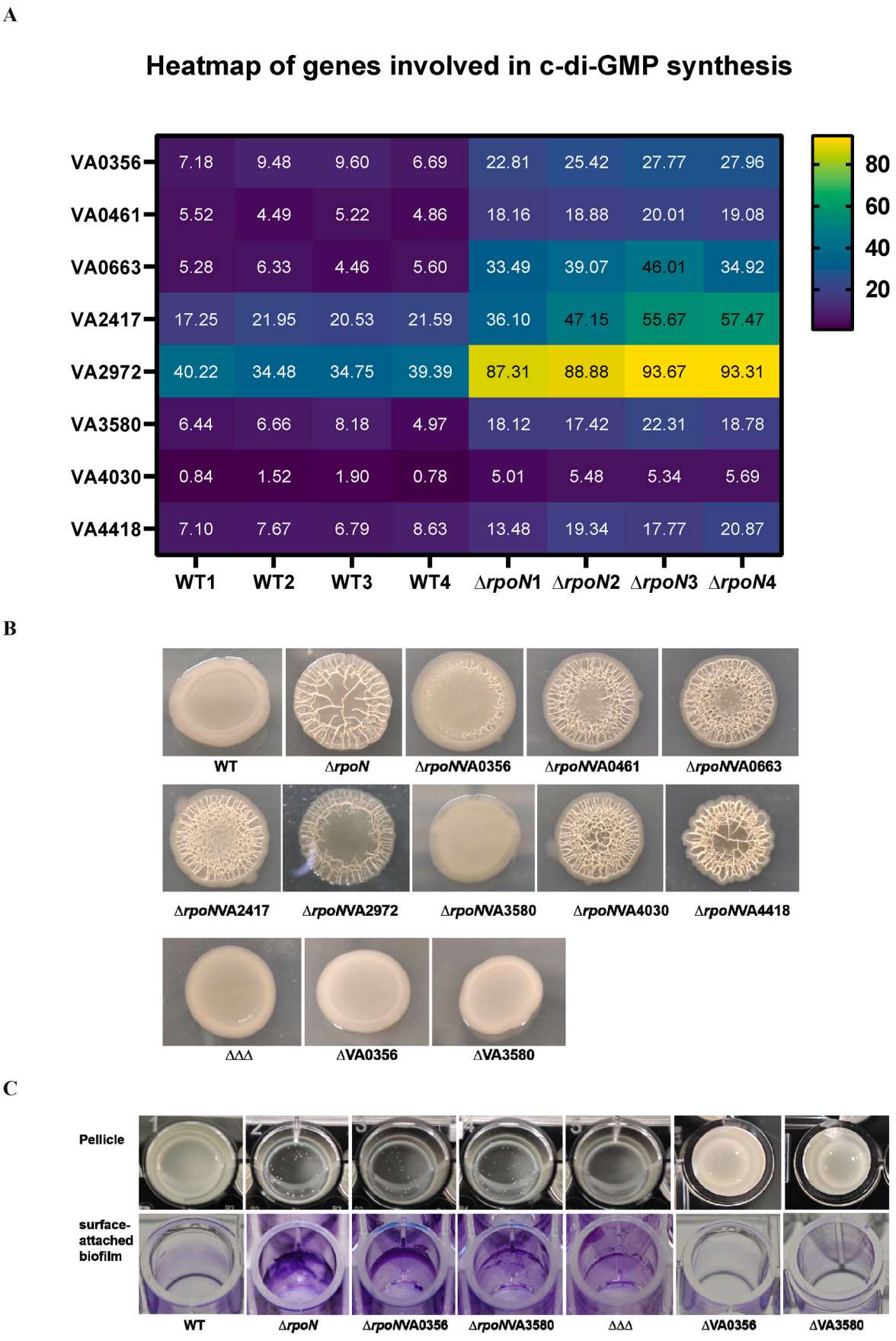

Fig. 3. Phenotypes associated with c-di-GMP. (A). Heat map of genes involving in c-di-GMP synthesis. The proximity to yellow indicated high transcript levels, while blue signified low. (B). Colony biofilms. The double-genes mutant strain was derived from eight genes encoding c-di-GMP synthetase which was up-regulated in the

transcriptome of Δ*rpoN* vs WT. Subsequently, based on the results from the double mutant strain, a triple gene mutant strain (ΔΔΔ) was further generated. To ensure experimental comprehensiveness, single-gene mutant strains (ΔVA0356 and ΔVA3580) were also constructed. (C). Pellicle biofilm formation and SB stained with crystal violet at 24 h. (D). Domain analysis of VA0356 was performed using software SMART (http://smart.embl-heidelberg.de/smart/set_mode.cgi?NORMAL=1). The predicted domains from left to right include the Transmembrane region (represented by a blue rectangle), dCache-1, PAS, PAC, and GGDEF. (E). A potential binding site for *rpoN* located in the upstream region of VA3579 and VA3580. Red square represented potential binding site on the genome, indicating transcription in the same direction as VA3579 and VA3580 (arrow direction). The predicted protein structural domains were shown below the genes. (F). The binding of *rpoN* to the putative binding site of VA3579 upstream by EMSA. The concentration of RpoN-protein and labeled DNA probe 2.142 mg/mL and 20.3 ng/μL, respectively. The upper band represented the protein-DNA binding complex. The lower band corresponds to the unbound DNA probe. (G) and (H) were quantification of c-di-GMP concentration and SB stained with crystal violet, respectively. Data were statistically analyzed using Prism 9 (GraphPad Software). Significance is expressed as follows:$^{ns}p>0.05$, $^{*}p<0.05$, $^{**}p<0.01$, $^{***}p<0.001$, and $^{****}p<0.0001$. (For interpretation of the references to color in this figure legend, the reader is referred to the Web version of this article.)

pyruvate kinase PykF (for detailed descriptions refer to Table S3).

The fusion protein VA3580 consisted of Tetratricopeptide (TPR) repeat and GGDEF region (Fig. 3E). VA3580 and its upstream gene VA3579 shared 16bp overlapping sequences. VA3579 was annotated as a protein containing three TRP regions (Fig. 3E). The primary function of TPR folds was to facilitate protein-protein interactions. Analysis of the surrounding regions revealed that VA3577-VA3585 exhibited consistent transcriptional orientation, with multiple genes having overlapping segments within them. Only VA3579 and VA3580 showed significant up-regulation at the transcript levels in Δ*rpoN* (for detailed descriptions refer to Table S3). A potential RpoN binding site TTGGCA-TAATTTGTGCTAT was predicted 256bp upstream of VA3579 (Fig. 3E), which was confirmed by EMSA assay (Fig. 3F). The intracellular concentration of c-di-GMP in Δ*rpoN* was significantly higher than that in WT and ΔΔΔ (Fig. 3G). However, the c-di-GMP content of Δ*rpoN*VA0356 and Δ*rpoN*VA0380 was lower than that of Δ*rpoN* but comparable to that of WT. Single-gene mutations (ΔVA0356 and ΔVA3580) exhibited similar effects on biofilm formation and intracellular c-di-GMP levels as observed in WT. Taken together, these findings suggested that RpoN can directly or indirectly regulate VA3580 and VA0356, respectively, thereby influencing intracellular c-di-GMP levels which subsequently affect biofilm formation.

3.5. Hypoxic metabolism is impaired in Δ*rpoN*

3.5.1. Δ*rpoN* preferentially survived at ALI

The growth curve during static culture showed that the growth capacity of Δ*rpoN* in liquid phase was significantly reduced compared to WT (Fig. 4A). The logarithmic growth phase of WT was 8 h at the early stage of the culture with a homogeneous turbid bacterial suspension, whereas measurement of absorbance in liquid medium showed that Δ*rpoN* grew slowly all the time with no discernible logarithmic period. The maximum biomass of WT and Δ*rpoN*, as reflected by the OD_{600} value, were 1.05 and 0.65, respectively, with the former being double the latter. During this process, all bacterial cells of Δ*rpoN* and Δ*rpoN*-derived strains tended towards the ALI, forming aggregates of cells with aerotaxis, with SB forming first, followed by PB (Fig. S3). The liquid phase was virtually devoid of bacteria and was incapable of forming a turbid bacterial solution (Figs. 2D and 3C).

To further investigate the relationship between Δ*rpoN*, oxygen, and biofilm formation, we applied low oscillation conditions (30 rpm) to Δ*rpoN*. This condition provided the bacteria with more available oxygen compared to static culture but did not limit biofilm formation due to severe agitation. After 12 h of incubation, Δ*rpoN* formed a robust, complete, and compact pellicle. The turbidity of the Δ*rpoN* bacterial solution was significantly enhanced compared to that of static culture (Fig. 4B). These findings suggested that increased oxygen can indeed improve the growth capacity and biofilm formation ability of Δ*rpoN*. In contrast, compared with shaking culture, the amount of available oxygen in static culture is limited, Δ*rpoN* was powerless to form a complete pellicle due to low cell concentration. We speculated that the absence of *rpoN* may impair hypoxic metabolism in *V. alginolyticus* leading to strong oxygenotaxis which explained why Δ*rpoN* gathered at the air-liquid interface (ALI) and formed a remarkable SB, even without *vps* gene involved in cannot destroy SB formation. Additionally, it was observed that SB exhibited a preferential formation over PB during the culture process. Consequently, it can be inferred that the aerobic substrate surface serves as a more suitable ecological niche for the survival and proliferation of Δ*rpoN*.

3.5.2. *rpoN* promotes acetaldehyde, ethanol dehydrogenase, and acetate kinase

Under insufficient oxygen, the formation of pyruvate into ethanol and lactic acid is an NAD^+ regeneration pathway, whereas the formation of acetate is the pathway of ATP production [40]. It has previously been reported in *V. cholerae* that the ethanol pathway cannot be compensated for by other NAD^+-producing branches [41]. Thus, pyruvate is catalyzed to ethanol and acetate is an important pathway under hypoxic conditions. According to the results of KEGG pathway enrichment analysis, the key genes involved in pyruvate metabolic pathway changed significantly between WT and Δ*rpoN*. Under oxygen-limited conditions, pyruvate is converted to acetyl-CoA by pyruvate dehydrogenase, which is then converted to acetyl phosphate (AcP) by phosphotransacetylase. In the three subsequent processes (i.e., conversion of AcP to acetate, acetate to acetaldehyde, and acetaldehyde to ethanol), the genes (e.g., VA4419, VA1349, and VA4352) encoding acetate kinase (ACK), aldehyde dehydrogenase (ALDH), and alcohol dehydrogenase (ADH) were all significantly inhibited in Δ*rpoN* (Fig. 4C). The enzyme activity assay showed that the catalytic efficiency of the three enzymes was significantly decreased in Δ*rpoN* (Fig. 4D). Although the catalytic efficiency of the three enzymes was not very high in WT, that of Δ*rpoN* was almost zero in 5 min. Therefore, Under conditions where the amount of oxygen available is insufficient, the conversion of pyruvate to ethanol was severely limited in Δ*rpoN*, and the fate of pyruvate was regulated by *rpoN*. The above data provide transcriptional and enzymatic evidence that the absence of *rpoN* renders *V. alginolyticus* unable to survive in hypoxic environments because of its inability to undergo pyruvate catabolism; in turn, it tends to colonize the ALI to form spectacular SB where more oxygen is available.

4. Discussion

rpoN is a global transcriptional regulatory factor that is widely distributed in *Vibrio* spp. and plays a key regulatory role in bacterial growth and pathogenesis [42]. *rpoN* has highly conserved functions among *Vibrio* spp. and enhances swimming motility, flagellar synthesis, and the type VI secretion system (T6SS) in *Vibrio* spp. [32–37]. Genome-wide association analysis in *E. coli* revealed non-random orientation and location of *rpoN* binding sites [43]. Over half (52 %) of the binding sites were located inside genes, situated more than 500 bp away from the gene start site. Furthermore, the inside genes binding sites exhibited transcription activity, functioning as promoters for downstream mRNA with unusually long 5′ UTRs. Mutations in these binding sites significantly reduced the transcription levels of the downstream genes. The previous reports have indicated that the regulation of *Vibrio* spp. VPS by *rpoN* was enhanced but not obligatory [11,15,19]. Furthermore, *rpoN* did not directly bind to the upstream region of the *vps* gene cluster. However, in *Pseudomonas stutzeri*, RpoN directly

D

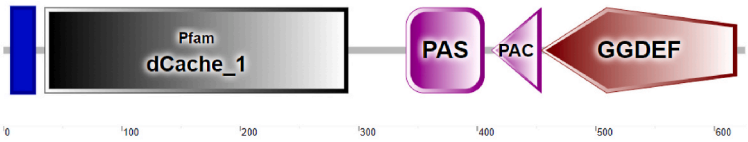

E

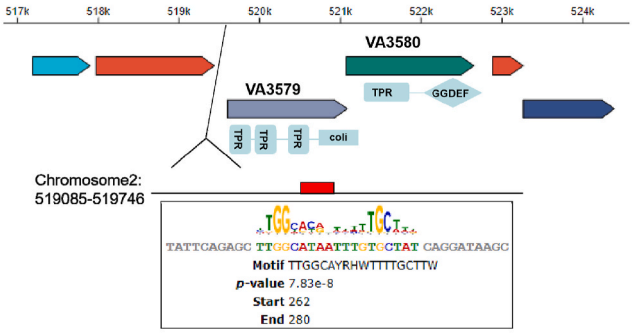

F

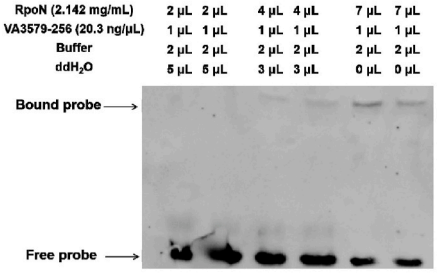

G

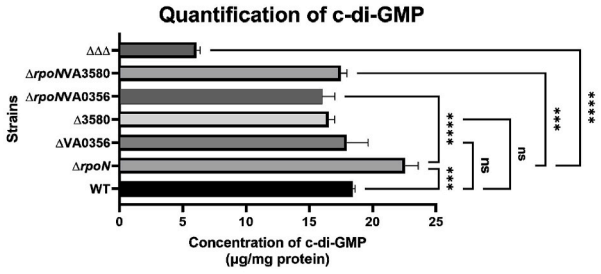

H

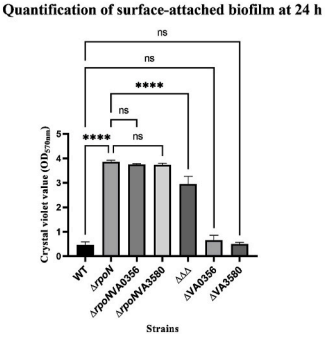

Fig. 3. (*continued*).

A

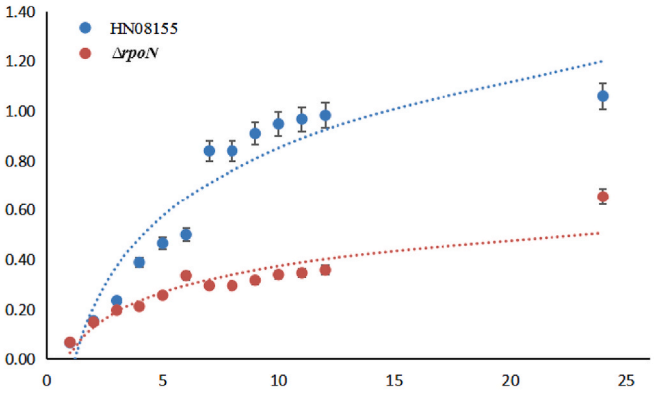

B

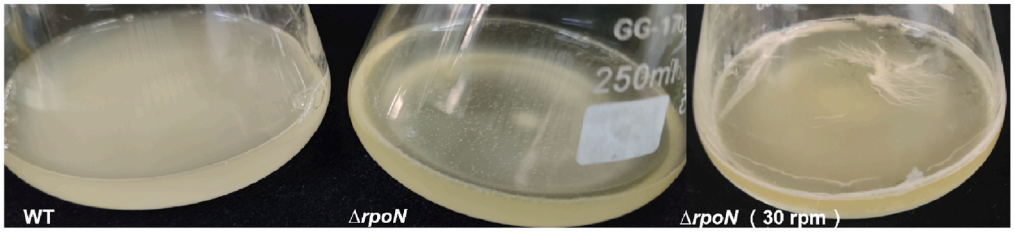

C

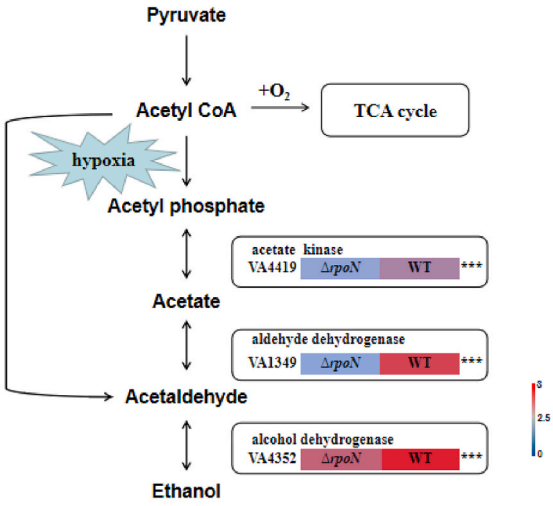

D

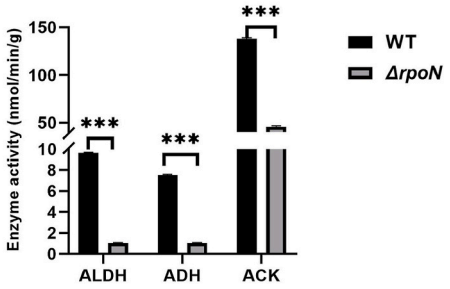

(caption on next page)

Fig. 4. RpoN regulates hypoxic metabolism in *V. alginolyticus* HN08155. (A). Growth curve in static culture. The blue and red dots represent WT and Δ*rpoN* respectively. The blue and red lines are trend lines in logarithms for the growth capacity of WT and Δ*rpoN*, respectively. Each group had five biological replicates. (B). Pellicle formation at the ALI. Strains were WT-static, Δ*rpoN*-static and Δ*rpoN*-30 rpm cultured in LB medium for 24 h. (C). Abridged edition of pyruvate metabolism pathway. The inside heatmaps indicate the abundance of gene transcripts in WT and Δ*rpoN*. The abundance of gene transcripts was expressed as $\log_{10}$-transformed mean FPKM values. Colors represent relative gene expression; the closer the color is to red, the higher the expression, and the closer the color is to blue, the lower the expression. Significantly altered genes compared to the WT were marked with an asterisk (***). (D) Enzyme activity assays. Changes in NADH, determined by light absorption at 340 nm, were detected within 5 min. Aldehyde dehydrogenase, ALDH; Alcohol dehydrogenase, ADH; Acetate kinase, ACK. *** indicates $p < 0.001$. (For interpretation of the references to color in this figure legend, the reader is referred to the Web version of this article.)

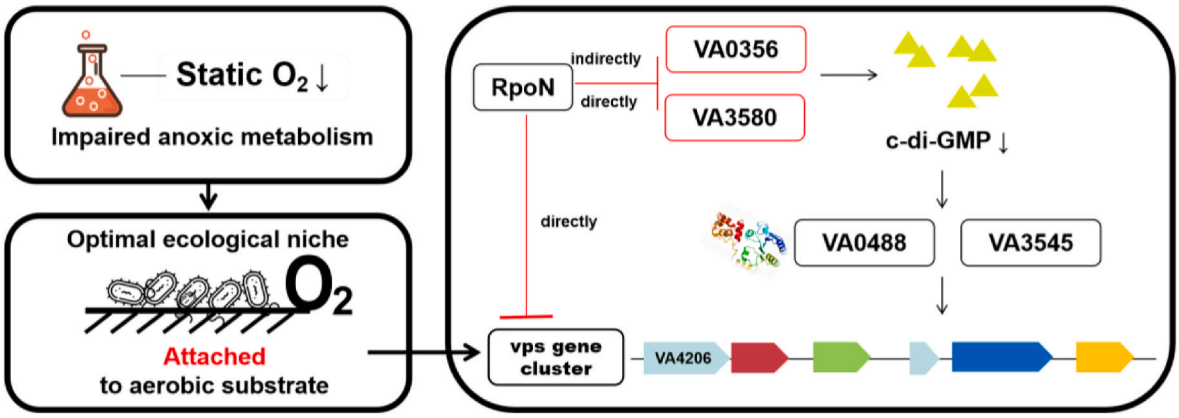

Fig. 5. Current model of the regulatory network connecting *rpoN*, c-di-GMP metabolism, oxygen-related metabolism and biofilm formation in *V. alginolyticus* HN08155. Arrows and horizontal bars indicate facilitation and inhibition, respectively. Both expolysaccharide synthesis and oxygen-related metabolism played crucial roles in Δ*rpoN* biofilm formation. *RpoN* affected expolysaccharide synthesis by directly regulating the *vps* gene cluster and c-di-GMP synthesis genes. Deletion of *rpoN* in *V. alginolyticus* resulted in impaired hypoxic metabolism, forcing the bacteria to rely solely on attachment to aerobic substrate surfaces for survival. See the text for further details.

binded to a 27 bp DNA region (CCGGAGA**GG**CACGGTCGGA**GC**AGGAGT) within the *pslA* promoter, thereby enhancing the expression of the *psl* gene cluster which encoded Psl represented the predominant exopolysaccharide present in the biofilm matrix [26]. In our study, although the presence of *rpoN* was determined to be non-essential for *V. alginolyticus vps* expression, it was observed that *rpoN* could exert an inhibitory effect on *vps* by directly binding at 1233bp upstream of VA4206-ATG. *V. alginolyticus* exhibited similarities to *Pseudomonas* rather than other *Vibrio* spp.

RpoN-RNAP bound to promoter DNA forms a closed complex that requires bacterial enhancer-binding proteins (bEBPs) to open and initiate transcription [17]. Classical bEBPs contain three conserved domains: an N-terminal receptor (REC) domain, a central AAA + domain involved in ATP hydrolysis and binding to *rpoN* (adenosine triphosphatase (ATPase) associated with multiple cellular activities), and a C-terminal helix-turn-helix DNA binding domain. Regulation of bEBP occurred through phosphorylation, ligand binding, and protein-protein interaction. Irrespective of the perception mechanism, negative regulation predominated in bEBPs regulation. VpsR is classified as an atypical EBP, based on its amino acid sequence homology. Although VpsR shares global homology with EBP, several functional residues are not conserved and have been mutated at both the GAFTGA (binding *rpoN*) and DE (hydrolyzed ATP) sites in *V. cholerae* [11]. In *V. alginolyticus* HN08155, the VpsR protein exhibited similarity to that in *V. cholerae*, with mutations observed at both the GAFTGA and DE sites, rendering it unable to interact with RpoN. Furthermore, no binding site for *rpoN* was identified in the upstream region of *vpsR*, however, mutation of *rpoN* led to a significant up-regulation of *vpsR*, suggesting *rpoN* indirect effected on *vpsR*. Both VpsR and VpsT served as effectors of c-di-GMP and are activated by c-di-GMP [21,22,44]. A high concentration of c-di-GMP is known to promote biofilm formation and inhibit flagella synthesis in bacteria. There are substantial quantity of redundant proteins involved in c-di-GMP turnover in *Vibrio* spp. [24], featuring distinct N-terminal signaling domains that enable sensitivity to a wide range of intracellular and extracellular cues [45]. It has been reported that the specific physical binding between the protein encoding DGCs and c-di-GMP receptor protein, along with negative feedback regulation through an autoinhibitory site (I-site) on the DGCs, ensures precise bacterial response to signaling factors [45]. In *V. alginolyticus* HN08155, the mutation of *rpoN* led to 8 DGCs-encoding genes upregulated. However, it was only the specific deletions of VA0356 and VA3580 that significantly impacted the Δ*rpoN* biofilm formation. Although colonies of Δ*rpoN*VA0356 and Δ*rpoN*VA3580 appeared relatively smooth at 24 h, extended incubation resulted in the development towards rugose colonies. Previous research has shown that the overexpression of DGCs, such asVA0356, VA1591 (*cdgM*), VA4033 (*dgcB*), and VA0088, along with other related enzymes, enhances biofilm formation [24]. This finding implies that partly genes encoding DGCs may have functional redundancy, allowing them to compensate for one another. Under varying environmental conditions, specific genes encoding DGCs are preferentially activated to modulate c-di-GMP levels. However, when these genes are deleted or disrupted, the remaining genes can step in to compensate for their absence, ensuring the continuation of essential bacterial physiological processes.

Moreover, the mechanism by which *rpoN* regulates biofilm formation varies among different *Vibrio* spp. [14], which is closely related to the fact that biofilm formation is mainly regulated by various environmental signals such as nutrients, osmolarity, oxygen concentration, and the frequency of influence by planktonic cells [8,46]. The ecological niche of each *Vibrio* species differs. Biofilm formation is an important strategy for occupying favorable ecological niches [47]. Under laboratory culture conditions, there are air-liquid interface (ALI) biofilms floating on the medium (i.e., pellicles), ALI biofilm rings attached to the wall (i.e., surface-attached biofilms, SB), submerged biofilms (attached to the wall and submerged in water), solid-liquid interface biofilms (bottom biofilms), and rugose colonies formed on the plate medium [7]. Although the initial regulatory synthesis of extracellular matrix components is programmed, biofilm formation is mainly governed by adaptive responses without a core set of biofilm genes [48]. Environmental factors in the niche affect the expression of the genes involved in biofilm formation. For example, extracellular matrix formation in *Bacillus subtilis* is redundantly regulated by four kinases, of which KinA and KinB act on

mature or aged sites, whereas KinC and KinD activate younger regions in rugose colonies. However, this regulation is absent during pellicle formation [49]. Our study showed that the VPS of *V. alginolyticus* regulates the formation of PB and rugose colony but cannot fully control the formation of SB in Δ*rpoN*. Although both mutant strains Δ*rpoN* and Δ*hapR* showed an increase in VPS, *hapR* is more effective in regulating pellicles, while *rpoN* has a stronger control on rugose colony formation in *V. alginolyticus* (Data not shown). Interestingly, the absence of *rpoN* in *B. cereus* ATCC 14579 had a similar tendency in colony morphology as *V. alginolyticus* HN08155, changing from the round shaped and wide-spread colonies (WT) to a characteristic dendritic (branched) colony morphology (Δ*rpoN*), whereas the trend of SB formation was completely reversed, lacking attachment ability at the ALI [50]. Therefore, although the stage of exopolysaccharide synthesis may be the same, gene regulation in the later stages of biofilm formation depends on the ecological environment.

It has previously been reported that *Pseudomonas aeruginosa* formed biofilms at the ALI, and that the medium below the liquid surface was transparent with almost no bacteria present, whereas a polysaccharide-deficient mutant strain (Δ*psl*Δ*pel*) formed a turbid bacterial suspension [8]. In *V. alginolyticus* HN08155, the deletion of *rpoN* resulted in the formation of an abnormally strong SB, and the liquid medium was clear, whereas the loss of VPS did not alter the formation of SB. The impaired hypoxic metabolism during static culture was the primary cause of the unusual SB of Δ*rpoN*, and the formation of SB was also superior to PB. Although the cell density of Δ*rpoN* in the liquid medium was low, it was also able to form visible submerged biofilms, suggesting that attachment to the substrate is an important survival strategy for *V. alginolyticus*. Δ*rpoN* attached itself to the wall at the ALI and obtained the most suitable ecological niche, where it survived and reproduced rapidly using the available nutrients and oxygen.

Vibrio spp. often experience extreme changes in their oxygen levels during natural and host infections [51]. Although multiple approaches existed for pyruvate metabolism under anoxic conditions, it appeared that every pathway was mediated by *rpoN* [40,43]. Pyruvate was converted to formate, and the activation of the formate hydrolyase (FHL) complex for hydrogen generation requires the involvement of the *rpoN*-dependent transcription activator *fhlA* [52]. The conversion of fumarate to succinate relied on the dicarboxylic acid transport system *dctABC*, which was regulated by another *rpoN*-dependent transcription activator *dctD* [53]. Furthermore, our study revealed a significant reduction in gene expression levels and enzyme activity of three enzymes (ALDH, ADH, and ACK) involved in converting pyruvic acid to ethanol under low oxygen conditions. Unfortunately, no potential binding sites for *rpoN* were found upstream of VA1349, VA4352, and VA4419. These findings suggested that *rpoN* played a crucial role in low oxygen metabolism in *Vibrio* spp. However, there was still insufficient evidence regarding specific metabolic pathways related to Δ*rpoN* in static LB medium under low oxygen condition. Various respiratory-related enzymes have been reported as essential for biofilm maturation [40]. In *V. vulnificus*, when exposed to dicarboxylic acids, *dctD2* directly interacts with EPS-II and EPS-III upstream regions to maximize mature biofilm promotion [54]. Therefore, understanding the relationship between *rpoN* regulation and respiratory/fermentation metabolism influencing biofilm formation can contribute towards comprehending the colonization mechanism and persistence of *V. alginolyticus* within host.

5. Conclusion

The *vps* gene cluster in *V. alginolyticus* Δ*rpoN* exerted complete control over the formation of rugose colony morphology and pellicle, while only partially contributing to SB. As a central regulator, *rpoN* governed biofilm formation through two regulatory pathways. Firstly, it directly bind to the upstream region of VA4206 to regulate the expression of *vps* gene cluster (VA4206-VA4196). Secondly, it directly and indirectly modulated VA3580 and VA0356, thereby affecting c-di-GMP concentration and subsequently influencing the expression of transcription regulators vpsR and VA3545. Under conditions promoting SB formation, *rpoN* was unable to survive below the liquid level due to significantly reduced activities of three catalytic enzymes (ACK, ADH and ALDH) involved in pyruvate metabolism. This suggested that Δ*rpoN* cannot thrive in low oxygen environments but tends to reproduce in ALI, a relatively high oxygen niche that contributed to SB formation. In conclusion, multiple factors contribute to the unusually strong biofilm phenotype observed in Δ*rpoN* (Fig. 5), including the transcription of key bacterial genes and the metabolic response induced by external environmental stimuli. In this study, we demonstrated *rpoN* plays a crucial role in hypoxic metabolism and biofilm formation, offering valuable insights into the survival strategies employed by V. alginolyticus in both marine environments and host organisms.

CRediT authorship contribution statement

Na Zhang: Writing – review & editing, Writing – original draft, Visualization, Validation, Supervision, Software, Resources, Project administration, Methodology, Investigation, Formal analysis, Data curation, Conceptualization. **Yanhua Zeng:** Writing – review & editing, Funding acquisition, Formal analysis. **Jiachengzi Ye:** Software, Methodology. **Chuancao Lin:** Software, Methodology, Formal analysis. **Xiaoxiao Gong:** Software, Methodology. **Hao Long:** Investigation, Funding acquisition. **Haimin Chen:** Funding acquisition. **Zhenyu Xie:** Writing – review & editing, Funding acquisition, Formal analysis, Data curation, Conceptualization.

Data availability

The original contributions presented in the study are included in the article, further inquiries can be directed to the corresponding author.

Declaration of competing interest

The authors declare that they have no known competing financial interests or personal relationships that could have appeared to influence the work reported in this original manuscript.

Acknowledgements

This work was supported by the National Natural Science Foundation of China (32260927, 32060835 and 32303063), Key Research and Development Program of Hainan Province (ZDYF2022XDNY349), Innovative research project of graduate students in Hainan Province (Qhys2022-125).

Appendix A. Supplementary data

Supplementary data to this article can be found online at https://doi.org/10.1016/j.bioflm.2024.100242.

Data availability

The data that has been used is confidential.

References

[1] Economopoulou A, Chochlakis D, Almpan MA, Sandalakis V, Maraki S, Tselentis Y, Psaroulaki A. Environmental investigation for the presence of Vibrio species following a case of severe gastroenteritis in a touristic island. Environ Sci Pollut Res Int 2017;24(5):4835–40. https://doi.org/10.1007/s11356-016-8231-7.

[2] DeAngelis CM, Saul-McBeth J, Matson JS. Vibrio responses to extracytoplasmic stress. Environ. Microbiol. Rep. 2018;10(5):511–21. https://doi.org/10.1111/1758-2229.12693.

[3] Baker-Austin C, Oliver JD, Alam M, Ali A, Waldor MK, Qadri F, Martinez-Urtaza J. *Vibrio* spp. infections. Nat Rev Dis Prim 2018;4(1):8. https://doi.org/10.1038/s41572-018-0005-8.

[4] Matamp N, Bhat SG. Phage endolysins as potential antimicrobials against multidrug resistant *Vibrio alginolyticus* and *Vibrio parahaemolyticus*: current status of research and challenges ahead. Microorganisms 2019;7(3):84. https://doi.org/10.3390/microorganisms7030084.

[5] Yildiz FH, Visick KL. Vibrio biofilms: so much the same yet so different. Trends Microbiol 2009;17(3):109–18. https://doi.org/10.1016/j.tim.2008.12.004.

[6] Fong JNC, Yildiz FH. Biofilm matrix proteins. Microbiol Spectr 2015;3(2). https://doi.org/10.1128/microbiolspec.MB-0004-2014. 10.1128/microbiolspec.MB-0004-2014.

[7] Armitano J, Méjean V, Jourlin-Castelli C. Gram-negative bacteria can also form pellicles. Environ. Microbiol. Rep. 2014;6(6):534–44. https://doi.org/10.1111/1758-2229.12171.

[8] Vaccari L, Molaei M, Niepa THR, Lee D, Leheny RL, Stebe KJ. Films of bacteria at interfaces. Adv Colloid Interface Sci 2017;247:561–72. https://doi.org/10.1016/j.cis.2017.07.016.

[9] Limoli DH, Jones CJ, Wozniak DJ. Bacterial extracellular polysaccharides in biofilm formation and function. Microbiol Spectr 2015;3(3). https://doi.org/10.1128/microbiolspec.MB-0011-2014. 10.1128/microbiolspec.MB-0011-2014.

[10] Laue H, Schenk A, Li H, Lambertsen L, Neu TR, Molin S, Ullrich MS. Contribution of alginate and levan production to biofilm formation by *Pseudomonas syringae*. Microbiology (Reading, England) 2006;152(Pt 10):2909–18. https://doi.org/10.1099/mic.0.28875-0.

[11] Hsieh ML, Waters CM, Hinton DM. VpsR directly activates transcription of multiple biofilm genes in *Vibrio cholerae*. J Bacteriol 2020;202(18):e00234. https://doi.org/10.1128/JB.00234-20. 20.

[12] Solano C, Echeverz M, Lasa I. Biofilm dispersion and quorum sensing. Curr Opin Microbiol 2014;18:96–104. https://doi.org/10.1016/j.mib.2014.02.008.

[13] Teschler JK, Nadell CD, Drescher K, Yildiz FH. Mechanisms underlying *Vibrio cholerae* biofilm formation and dispersion. Annu Rev Microbiol 2022;76:503–32. https://doi.org/10.1146/annurev-micro-111021-053553.

[14] Zhang N, Zhang S, Ren W, Gong X, Long H, Zhang X, Cai X, Huang A, Xie Z. Roles of *rpoN* in biofilm formation of *Vibrio alginolyticus* HN08155 at different cell densities. Microbiol Res 2021;247:126728. https://doi.org/10.1016/j.micres.2021.126728.

[15] Tague JG, Hong J, Kalburge SS, Boyd EF. Regulatory small RNA Qrr2 is expressed independently of sigma factor-54 and can function as the sole qrr small RNA to control quorum sensing in *Vibrio parahaemolyticus*. J Bacteriol 2022;204(1):e0035021. https://doi.org/10.1128/JB.00350-21.

[16] Yu C, Yang F, Xue D, Wang X, Chen H. The regulatory functions of σ54 factor in phytopathogenic bacteria. Int J Mol Sci 2021;22(23):12692. https://doi.org/10.3390/ijms222312692.

[17] Hartman CE, Samuels DJ, Karls AC. Modulating *Salmonella Typhimurium*'s response to a changing environment through bacterial enhancer-binding proteins and the RpoN regulon. Front Mol Biosci 2016;3:41. https://doi.org/10.3389/fmolb.2016.00041.

[18] Yildiz FH, Liu XS, Heydorn A, Schoolnik GK. Molecular analysis of rugosity in a *Vibrio cholerae* O1 El Tor phase variant. Mol Microbiol 2004;53(2):497–515.

[19] Cheng AT, Zamorano-Sánchez D, Teschler JK, Wu D, Yildiz FH. NtrC Adds a new node to the complex regulatory network of biofilm formation and vps expression in *Vibrio cholerae*. J Bacteriol 2018;200(15):e00025. https://doi.org/10.1128/JB.00025-18. 18.

[20] Hsieh ML, Hinton DM, Waters CM. VpsR and cyclic di-GMP together drive transcription initiation to activate biofilm formation in Vibrio cholerae. Nucleic Acids Res 2018;46(17):8876–87. https://doi.org/10.1093/nar/gky606.

[21] Guest T, Haycocks JRJ, Warren GZL, Grainger DC. Genome-wide mapping of *Vibrio cholerae* VpsT binding identifies a mechanism for c-di-GMP homeostasis. Nucleic Acids Res 2022;50(1):149–59. https://doi.org/10.1093/nar/gkab1194.

[22] Chakrabortty T, Roy Chowdhury S, Ghosh B, Sen U. Crystal structure of VpsR revealed novel dimeric architecture and c-di-GMP binding site: mechanistic implications in oligomerization, ATPase activity and DNA binding. J Mol Biol 2022;434(2):167354. https://doi.org/10.1016/j.jmb.2021.167354.

[23] Beyhan S, Bilecen K, Salama SR, Casper-Lindley C, Yildiz FH. Regulation of rugosity and biofilm formation in *Vibrio cholerae*: comparison of VpsT and VpsR regulons and epistasis analysis of *vpsT, vpsR*, and *hapR*. J Bacteriol 2007;189(2):388–402. https://doi.org/10.1128/JB.00981-06.

[24] Gong XX, Zeng YH, Chen HM, Zhang N, Han Y, Long H, Xie ZY. Bioinformatic and functional characterization of cyclic-di-GMP metabolic proteins in *Vibrio alginolyticus* unveils key diguanylate cyclases controlling multiple biofilm-associated phenotypes. Front Microbiol 2023;14:1258415. https://doi.org/10.3389/fmicb.2023.1258415.

[25] Waters CM, Lu W, Rabinowitz JD, Bassler BL. Quorum sensing controls biofilm formation in *Vibrio cholerae* through modulation of cyclic di-GMP levels and repression of *vpsT*. J Bacteriol 2008;190(7):2527–36. https://doi.org/10.1128/JB.01756-07.

[26] Shang L, Yan Y, Zhan Y, Ke X, Shao Y, Liu Y, Yang H, Wang S, Dai S, Lu J, Yan N, Yang Z, Lu W, Liu Z, Chen S, Elmerich C, Lin M. A regulatory network involving Rpo, Gac and Rsm for nitrogen-fixing biofilm formation by *Pseudomonas stutzeri*. NPJ Biofilms Microbiome. 2021;7(1):54. https://doi.org/10.1038/s41522-021-00230-7.

[27] Bartosik AA, Glabski K, Jecz P, Mikulska S, Fogtman A, Koblowska M, Jagura-Burdzy G. Transcriptional profiling of ParA and ParB mutants in actively dividing cells of an opportunistic human pathogen *Pseudomonas aeruginosa*. PLoS One 2014;9(1):e87276. https://doi.org/10.1371/journal.pone.0087276.

[28] Pisithkul T, Schroeder JW, Trujillo EA, Yeesin P, Stevenson DM, Chaiamarit T, Coon JJ, Wang JD, Amador-Noguez D. Metabolic remodeling during biofilm development of *Bacillus subtilis*. mBio 2019;10(3):e00623. https://doi.org/10.1128/mBio.00623-19. 19.

[29] Barrientos-Moreno L, Molina-Henares MA, Ramos-González MI, Espinosa-Urgel M. Role of the transcriptional regulator ArgR in the connection between arginine metabolism and c-di-GMP signaling in *Pseudomonas putida*. Appl Environ Microbiol 2022;88(7):e0006422. https://doi.org/10.1128/aem.00064-22.

[30] Yang S, Peng Q, Zhang Q, Yi X, Choi CJ, Reedy RM, Charkowski AO, Yang CH. Dynamic regulation of GacA in type III secretion, pectinase gene expression, pellicle formation, and pathogenicity of *Dickeya dadantii* (*Erwinia chrysanthemi* 3937). MPMI Mol. Plant. Microbe Interact. 2008;21(1):133–42. https://doi.org/10.1094/MPMI-21-1-0133.

[31] Visick KL, Quirke KP, McEwen SM. Arabinose induces pellicle formation by *Vibrio fischeri*. Appl Environ Microbiol 2013;79(6):2069–80. https://doi.org/10.1128/AEM.03526-12.

[32] Dong TG, Mekalanos JJ. Characterization of the RpoN regulon reveals differential regulation of T6SS and new flagellar operons in *Vibrio cholerae* O37 strain V52. Nucleic Acids Res 2012;40(16):7766–75. https://doi.org/10.1093/nar/gks567.

[33] Gu D, Zhang Y, Wang K, Li M, Jiao X. Characterization of the RpoN regulon reveals the regulation of motility, T6SS2 and metabolism in *Vibrio parahaemolyticus*. Front Microbiol 2022;13:1025960. https://doi.org/10.3389/fmicb.2022.1025960.

[34] Hao B, Mo ZL, Xiao P, Pan HJ, Lan X, Li GY. Role of alternative sigma factor 54 (RpoN) from *Vibrio anguillarum* M3 in protease secretion, exopolysaccharide production, biofilm formation, and virulence. Appl Microbiol Biotechnol 2013;97(6):2575–85. https://doi.org/10.1007/s00253-012-4372-x.

[35] Tsang J, Hoover TR. Themes and variations: regulation of RpoN-dependent flagellar genes across diverse bacterial species. Sci Tech Rep 2014;2014:681754. https://doi.org/10.1155/2014/681754.

[36] Manera K, Caro F, Li H, Pei TT, Hersch SJ, Mekalanos JJ, Dong TG. Sensing of intracellular Hcp levels controls T6SS expression in *Vibrio cholerae*. Proc Natl Acad Sci USA 2021;118(25):e2104813118. https://doi.org/10.1073/pnas.2104813118.

[37] Sheng L, Gu D, Wang Q, Liu Q, Zhang Y. Quorum sensing and alternative sigma factor RpoN regulate type VI secretion system I (T6SSVA1) in fish pathogen Vibrio alginolyticus. Arch Microbiol 2012;194(5):379–90. https://doi.org/10.1007/s00203-011-0780-z.

[38] Kimbrough JH, Cribbs JT, McCarter LL. Homologous c-di-GMP-Binding scr transcription factors orchestrate biofilm development in *Vibrio parahaemolyticus*. J Bacteriol 2020;202(6):e00723. https://doi.org/10.1128/JB.00723-19. 19.

[39] Ante VM, Bina XR, Howard MF, Sayeed S, Taylor DL, Bina JE. *Vibrio cholerae leuO* transcription is positively regulated by ToxR and contributes to bile resistance. J Bacteriol 2015;197(22):3499–510. https://doi.org/10.1128/JB.00419-15.

[40] Bueno E, Pinedo V, Cava F. Adaptation of *Vibrio cholerae* to hypoxic environments. Front Microbiol 2020;11:739. https://doi.org/10.3389/fmicb.2020.00739.

[41] Bueno E, Sit B, Waldor MK, Cava F. Anaerobic nitrate reduction divergently governs population expansion of the enteropathogen *Vibrio cholerae*. Nat. Microbiol. 2018;3:1346. https://doi.org/10.1038/s41564-018-0253-0.

[42] Whitaker WB, Richards GP, Boyd EF. Loss of sigma factor RpoN increases intestinal colonization of *Vibrio parahaemolyticus* in an adult mouse model. Infect Immun 2014;82(2):544–56. https://doi.org/10.1128/IAI.01210-13.

[43] Bonocora RP, Smith C, Lapierre P, Wade JT. Genome-scale mapping of *Escherichia coli* σ54 reveals widespread, conserved intragenic binding. PLoS Genet 2015;11(10):e1005552. https://doi.org/10.1371/journal.pgen.1005552.

[44] Shikuma NJ, Fong JC, Yildiz FH. Cellular levels and binding of c-di-GMP control subcellular localization and activity of the *Vibrio cholerae* transcriptional regulator VpsT. PLoS Pathog 2012;8(5):e1002719. https://doi.org/10.1371/journal.ppat.1002719.

[45] Dahlstrom KM, Giglio KM, Sondermann H, O'Toole GA. The inhibitory site of a diguanylate cyclase is a necessary element for interaction and signaling with an effector protein. J Bacteriol 2016;198(11):1595–603. https://doi.org/10.1128/JB.00090-16.

[46] Yan J, Nadell CD, Stone HA, Wingreen NS, Bassler BL. Extracellular-matrix-mediated osmotic pressure drives *Vibrio cholerae* biofilm expansion and cheater exclusion. Nat Commun 2017;8(1):327. https://doi.org/10.1038/s41467-017-00401-1.

[47] Martín-Rodríguez AJ. Respiration-induced biofilm formation as a driver for bacterial niche colonization. Trends Microbiol 2023;31(2):120–34. https://doi.org/10.1016/j.tim.2022.08.007.

[48] Tolker-Nielsen T. Biofilm development. Microbiol Spectr 2015;3(2). https://doi.org/10.1128/microbiolspec.MB-0001-2014.

[49] McLoon AL, Kolodkin-Gal I, Rubinstein SM, Kolter R, Losick R. Spatial regulation of histidine kinases governing biofilm formation in *Bacillus subtilis*. J Bacteriol 2011;193(3):679–85. https://doi.org/10.1128/JB.01186-10.

[50] Hayrapetyan H, Tempelaars M, Nierop Groot M, Abee T. *Bacillus cereus* ATCC 14579 RpoN (sigma 54) is a pleiotropic regulator of growth, carbohydrate metabolism, motility, biofilm formation and toxin production. PLoS One 2015;10(8):e0134872. https://doi.org/10.1371/journal.pone.0134872.

[51] Bueno E, Sit B, Waldor MK, Cava F. Genetic dissection of the fermentative and respiratory contributions supporting *Vibrio cholerae* hypoxic growth. J Bacteriol 2020;202(24):e00243. https://doi.org/10.1128/JB.00243-20. 20.

[52] Hopper S, Korsa I, Böck A. The nucleotide concentration determines the specificity of in vitro transcription activation by the sigma 54-dependent activator FhlA.

J Bacteriol 1996;178(1):199–203. https://doi.org/10.1128/jb.178.1.199-203.1996.

[53] Lee JH, Hoover TR. Protein crosslinking studies suggest that *Rhizobium meliloti* C4-dicarboxylic acid transport protein D, a sigma 54-dependent transcriptional activator, interacts with sigma 54 and the beta subunit of RNA polymerase. Proc Natl Acad Sci USA 1995;92(21):9702–6. https://doi.org/10.1073/pnas.92.21.9702.

[54] Kang S, Park H, Lee KJ, Lee KH. Transcription activation of two clusters for exopolysaccharide biosynthesis by phosphorylated DctD in *Vibrio vulnificus*. Environ Microbiol 2021;23(9):5364–77. https://doi.org/10.1111/1462-2920.15636.